Black hole accretion discs in the canonical low-hard state

R. C. Reis,[1]* A. C. Fabian[1] and J. M. Miller[2]

[1]*Institute of Astronomy, Madingley Road, Cambridge CB3 0HA*
[2]*Department of Astronomy, University of Michigan, 500 Church Street, Ann Arbor, MI 48109, USA*

ABSTRACT

Stellar mass black holes in the low-hard state may hold clues to jet formation and basic accretion disc physics, but the nature of the accretion flow remains uncertain. A standard thin disc can extend close to the innermost stable circular orbit, but the inner disc may evaporate when the mass accretion rate is reduced. Blackbody-like continuum emission and dynamically broadened iron emission lines provide independent means of probing the radial extent of the inner disc. Here, we present an X-ray study of eight black holes in the low-hard state. A thermal-disc continuum with a colour temperature consistent with $L \propto T^4$ is clearly detected in all eight sources, down to $\approx 5 \times 10^{-4} L_{\mathrm{Edd}}$. In six sources, disc models exclude a truncation radius larger than $10 r_{\mathrm{g}}$. Iron Kα fluorescence line emission is observed in half of the sample, down to luminosities of $\approx 1.5 \times 10^{-3} L_{\mathrm{Edd}}$. Detailed fits to the line profiles exclude a truncated disc in each case. If strong evidence of truncation is defined as (1) a non-detection of a broad iron line and (2) an inner disc temperature much cooler than expected from the $L \propto T^4$ relation, none of the spectra in this sample offers strong evidence of disc truncation. This suggests that the inner disc may evaporate at or below $\approx 1.5 \times 10^{-3} L_{\mathrm{Edd}}$.

Key words: accretion, accretion discs.

1 INTRODUCTION

The innermost regions of accreting black holes and the underlying physics of the accretion process can be successfully studied using the X-ray spectra of black hole binaries (BHBs). Over the past years, such studies have revealed that Galactic black hole binaries (GBHBs) radiate in various distinct spectral states characterized by the relative strength of their soft and hard X-ray emission (McClintock & Remillard 2006).

The X-ray spectrum of BHB systems in their low-hard state is dominated by a power law with relatively low luminosity ($\leq 0.05 L_{\mathrm{Edd}}$; Maccarone 2003), a photon index Γ in the range ≈ 1.4–2 and an exponential cut-off at about 100 keV. This is in contrast with the high-soft state, where the spectrum is dominated by a quasi-blackbody component with a characteristic temperature of ~ 1 keV, and the highly luminous very-high state ($L \approx L_{\mathrm{Edd}}$) with a power-law component having a flux comparable to that of the soft blackbody. In the latter cases, the power law does not show evidence for a high-energy roll over. Superimposed on the continuum is the presence of various reflection features (Ross & Fabian 1993; Miller 2007) with the dominant component being the Fe–Kα emission line. In the inner regions of the accretion flow, the reflection spectrum appears blurred due to the combination of various relativistic effects. The degree of gravitational blurring is strongly dependent on the inner radius of the reflecting material (Fabian et al. 1989; Laor 1991).

Theoretically, the soft, quasi-blackbody component observed in the high-soft and very high state is generally agreed to originate in a standard, optically thick, geometrically thin accretion disc (Shakura & Sunyaev 1973) extending to the innermost stable circular orbit (ISCO). For a non-rotating, Schwarzschild, black hole, this radius is equal to $6 r_{\mathrm{g}}$ where $r_{\mathrm{g}} = GM/c^2$, and decreases to $\approx 1.2 r_{\mathrm{g}}$ for a maximally rotating, Kerr black hole (Thorne 1974). The power-law component dominating the X-ray spectra in the low-hard state, on the other hand, is believed to be produced by the inverse Compton scattering of soft photons in a thermal, optically thin region (Shapiro, Lightman & Eardley 1976; Sunyaev & Titarchuk 1980). However, there is no general consensus on the geometry of this optically thin region. In the accretion disc–corona model, the hard power law comes from either a patchy corona, possibly powered by magnetic flares (Beloborodov 1999; Di Matteo, Celotti & Fabian 1999; Merloni, Di Matteo & Fabian 2000; Merloni & Fabian 2001) or the base of a centrally located jet (Merloni & Fabian 2002; Markoff & Nowak 2004; Markoff, Nowak & Wilms 2005). In both the cases, the thin accretion disc extends close to the ISCO. An alternative model has the thin disc truncated at large distances from the black hole (Narayan & Yi 1995; Esin, McClintock & Narayan 1997) with the central region replaced by an advection-dominated accretion flow (ADAF) where, in some instances, material may condense out of this ADAF to maintain a further inner optically thick disc (Liu et al. 2007; Taam et al. 2008).

*E-mail: rcr36@ast.cam.ac.uk

In both interpretations for the geometry of the accretion disc in the low-hard state, it is expected that the thermal-disc component will have a low effective temperature. The low-mass accretion rates, and corresponding low luminosity observed in systems in the low-hard state implies a peak disc temperature <0.4 keV. In the case of a geometrically thin disc extending close to the ISCO, this temperature closely follows the $L \propto T^4$ relation. The expected temperature departs dramatically from this relation when the disc is truncated at the distances predicted by the ADAF models (see e.g. McClintock et al. 2001). A thermal component has been observed in a number of sources in the low-hard state. In particular, *XMM–Newton/Rossi X-ray Timing Explore* (*RXTE*) observations of GX 339−4 (Miller et al. 2006; Reis et al. 2008; Tomsick et al. 2008) and Swift J1753.5−0.127 (Miller, Homan & Miniutti 2006; Reis, Miller & Fabian 2009) as well as *Chandra* observation of XTE J1118+480 (Reis, Miller & Fabian 2009) have shown that the accretion disc in these sources are consistent with extending close to the ISCO. Evidence for the disappearance of this component has usually been the result of observations made with *RXTE* which lacks the low-energy coverage.

As mentioned above, a further feature in the X-ray spectra of BHBs are the various reflection signatures associated with the reprocessing of hard radiation by the cool accretion disc. The most prominent of these features is often the broad, skewed Fe Kα line observed in a number of BHBs (Miller 2007, 2009), Seyfert galaxies (Tanaka et al. 1995; Fabian et al. 2009) and accreting neutron stars (Cackett et al. 2008; Reis, Fabian & Young 2009). New fits to some ultraluminous X-ray sources (Caballero-Garcia & Fabian 2009) spectra suggest that a disc reflection may also be observed, though more sensitive spectra are needed to confirm this possibility. The strength of the reflection features can be typified by the equivalent width of the iron Kα line, $W_{K\alpha}$, which is expected to correlate linearly with the reflection fraction $R = \Omega/2\pi$, where Ω is defined as the solid angle covered by the accretion disc as viewed from the hard X-ray source. George & Fabian (1991) have shown that for a neutral accretion disc with solar abundances the reflection fraction closely follows $R \approx W_{K\alpha}/180$ eV. For stellar mass black holes in the low-hard state, R is observed to be below ~ 1. This 'weak' reflection can be interpreted as either a recession in the accretion disc, as in the ADAF interpretation (Esin et al. 1997), a highly ionized inner disc (Ross, Fabian & Young 1999) or mildly relativistic motion of the hot corona away from the disc (Beloborodov 1999). Using the latter model, Beloborodov showed that reflection fractions as low as ≈ 0.3 can be obtained in the low-hard state without invoking disc truncation.

In the following sections, we will present a systematic analysis of a sample of eight stellar mass BHBs in the low-hard state with the goal of better understanding the accretion disc and flow geometry of such systems. We find that for the sources observed in this work the accretion discs are consistent with extending close to the ISCO and suggest a set of observational criteria for the support of disc truncation. We start in Section 2 with an introduction to the various systems investigated. This is then followed by a detailed analyses of the property of the thermal component (Sections 3.1–3.4) and the reflection component (Section 3.5). Our results are summarized in Section 4.

2 OBSERVATIONS AND DATA REDUCTION

Our aim is to present a selection of high-quality spectra of various X-ray binaries in the low-hard state. In such a state, the temperature

of the accretion disc is usually observed to be below ≈ 0.4 keV and for this reason a strong requirement of our selection is that the data extend to a similar energy range. Observations made *solely* with the *RXTE* are thus not used in this work due to its low energy cut-off of approximately 3 keV. The bulk of the work presented here utilizes observations made with either *XMM–Newton* or *Suzaku*, with two further sources observed with *Chandra* and *Swift*. In what follows, we introduce the various sources which meet this criterion and describe the observations and data reduction in detail.

2.1 GX 339−4

GX 339−4 is a dynamically constrained BHB located at a distance of 8 ± 2 kpc (Zdziarski & Gierlinski 2004). Although its mass is not yet known, it is likely that GX 339−4 is amongst the more massive of the stellar mass black hole sources. The mass function of the system has been constrained to $\approx 6\,M_\odot$ (Hynes et al. 2003 and Muñoz-Darias, Casares & Martínez-Pais 2008) and results derived from radio observations suggests a low ($\theta \leq 30°$) inclination for the inner disc (Gallo et al. 2004). Similar low inclinations have also been found when modelling the reflection features present in the spectrum of GX 339−4 in outburst (Miller et al. 2004). The apparent low inner disc inclination mentioned above does not necessarily imply a massive ($>30\,M_\odot$) stellar mass black hole since it is possible that the inner disc is warped similarly to that observed in GRO J1655−40 (Martin, Tout & Pringle 2008) and V4641 Sgr (Martin, Reis & Pringle 2008). For the purpose of this work, we assume a black hole mass in the range of 10–$20\,M_\odot$ and an inner disc inclination between $10°$ and $30°$. We note here that throughout this paper we will adopt the largest range for the physical parameters (mass, distance and inclination) available in the literature for the various sources, unless the parameters have been well constrained.

Prior analyses of GX 339−4 in both the very-high (Miller et al. 2004) and intermediate (Miller et al. 2008) state have shown that the accretion disc extends close to $2r_g$ in those states. A similar conclusion has been reached by jointly fitting the reflection features present in the *XMM–Newton* spectra of both the low-hard and the very high state (Reis et al. 2008). In this work, the low-hard state spectrum of GX 339−4 described in Miller et al. (2004) is reanalysed using the more stringent reduction procedure detailed in Reis et al. (2008). We restrict our spectral analyses of the *XMM–Newton* EPIC–MOS data to the 0.5–10.0 keV energy range. The simultaneous *RXTE* PCA spectrum is fitted in the standard 3.0–25.0 keV energy range with 0.6 per cent systematic error and an edge at 4.78 keV ($\tau = 0.1$) to account for a strong Xe L absorption feature. The HXTE spectrum is fitted in the 25.0–100 keV range. When fitting the *RXTE* spectra along with that of *XMM–Newton*, a joint fit is achieved by allowing a normalization constant to float between the various spectra. All parameters were tied between observations unless stated otherwise. XSPEC v 12.5.0 (Arnaud 1996) was used to analyse all spectra presented in this paper. The quoted errors correspond to a 90 per cent confidence level for one parameter of interest unless stated otherwise.

2.2 XTE J1650−500

Optical observations have constrained the mass function of XTE J1650−500 (hereafter J1650) to $2.73 \pm 0.56\,M_\odot$ (Orosz et al. 2004). Together with a lower limit on the inclination of $50° \pm 3°$, this sets an upper limit to the mass of the central source of approximately $7.3\,M_\odot$. A recent analysis made by Shaposhnikov

& Titarchuk (2009) has placed a strong constraint on the mass of the central black hole of $9.7 \pm 1.6 \, M_\odot$ based on the scaling properties of quasi-periodic oscillations. The discrepancy between their results and that of Orosz et al. (2004) is attributed to a possible misclassification of the spectral class of the optical companion. Due to the uncertainty in the mass of J1650, we conservatively assume that it lies between 5.3 and $11.3 \, M_\odot$. The distance to J1650 has recently been estimated at 2.6 ± 0.7 kpc (Homan et al. 2006).

XMM–Newton observed J1650 during the transition from the low-hard to the very high state in 2001 (Miller et al. 2002). The source was mistakenly identified as being in the very-high state due to the presence of an unusually strong (at the time) iron line emission. However, the cold (≈ 0.3 keV) thermal component and low luminosity likely place the observation in a rising phase of the low-hard state (see e.g. Rossi et al. 2005). The presence of a broad, asymmetric Fe emission line led Miller et al. to suggest that the black hole in J1650 is rapidly rotating. This was later confirmed by Miniutti, Fabian & Miller (2004) using *BeppoSAX* observations taken both before and after that of *XMM–Newton*. Contrary to this interpretation, Done & Gierlinski (2006) showed that the bright, low-hard state, *BeppoSAX* observation is also consistent with a disc truncated at ~ 10–$20 r_g$ if there is resonance iron K absorption from an outflow disc wind with a velocity of $\approx 0.15c$.

Here, we analyse the same *XMM–Newton* EPIC–pn observation described in Miller et al. (2002). The source was observed in the 'burst' mode with the 'thin' optical filter in place. The spectrum was extracted using a box region centred on the source with a 20 pixel width. Background events were extracted from a 10 pixel wide box adjacent to the source. Single and double events were included in the analysis. Response files were created in the standard way using the tools RMFGEN and ARFGEN. The FTOOL GRPPHA was used to require at least 20 counts per bin in all *XMM–Newton* observations presented in this paper. We restrict our study of the *XMM–Newton* EPIC–pn data to the 0.6–10.0 keV energy range.

2.3 Cygnus X-1

Cygnus X-1 (hereafter Cyg X-1) is amongst the better known and studied stellar mass black holes. Having been the first object generally recognized as a black hole (Tananbaum et al. 1972), it has received considerable attention. The distance to the source was very early estimated at 2 kpc (Murdin & Webster 1971). This has been confirmed more recently by Massey, Johnson & Degioia-Eastwood (1995) where a distance of 2.1 ± 0.1 kpc is found. The orbital inclination of the system is thought to be in the range of $25°$–$50°$ (Gierlinski et al. 1999). The uncertainty in this value follows the fact that the accretion disc in Cyg X-1 is thought to be precessing (Stirling et al. 2001; Romero, Kaufman Bernado & Mirabel 2002) with an average angle to the line of sight of $\sim 30°$ (Fender 2001). The mass of the black hole is also highly uncertain, partially due to the uncertainty in the inclination. Although it is generally assumed to be close to $10 \, M_\odot$, its value has been found by various authors to range from 7 to $25 \, M_\odot$ (e.g. Ziolkowski 2005; Shaposhnikov & Titarchuk 2009).

Young et al. (2001) showed that the various spectra of Cyg X-1 in both the low-hard and the high-soft state are consistent with the relativistic blurring of a thin, ionized accretion disc extending close to the ISCO. This interpretation was later challenged by Barrio, Done & Nayakshin (2003). Using the high-energy coverage of *RXTE*, the authors were unsuccessful in measuring the high-energy break assumed to be characteristic of the ionized accretion

disc model,[1] and thus argued for a truncated disc interpretation of the spectra.

Makishima et al. (2008) observed the low-hard state of Cyg X-1 in 2005 October with *Suzaku*. Although the data suffered heavily from both pile up and telemetry saturation, the authors found the presence of a strong soft component with a temperature of ≈ 0.19 keV which was associated with an accretion disc extending to within ≈ 250 km. Assuming a mass of $10 \, M_\odot$, this is approximately $16 r_g$. We report on two recent *Suzaku* observations where the effect of pile-up is less prominent.

Cyg X-1 was observed with *Suzaku* on two occasions on 2009 April 8 (Obs ID 404075020; hereafter Obs 1) and April 14 (Obs ID 404075030; hereafter Obs 2) for approximately 50 and 33 ks, respectively. The three operating detectors constituting the X-ray Imaging Spectrometer (XIS; Koyama et al. 2007) were operated in the 'burst' clock mode in both observations and employed the '1/4 window' mode. The front illuminated (FI) detectors (XIS0 and XIS3) were operated in the 2×2 and 3×3 editing mode, whereas the back illuminated (BI) detector (XIS1) was operated in the 3×3 editing mode only. A total FI exposure of ≈ 10.7 and ≈ 8.6 ks for Obs 1 and 2, respectively, were available for each XIS camera. The corresponding BI exposures were 5.3 and 4.4 ks. Using the latest HEASOFT v6.6.2 software package, we reprocessed the data from the version 2 processing following the Suzaku Data Reduction Guide.[2] We started by creating new cleaned event files using the tool 'XISPI' and the script 'XISREPRO' as well as the associated screening criteria files. XSELECT was then used to extract spectral products. In both observations, source events were extracted from a region composed of the intersection of a rectangle of size 150×1024 pixels with an annulus having 30 and 200 pixel inner and outer radius, respectively. Background events were extracted from a circular region with a radius of 90 pixel away from the source. We used the script 'XISRESP'[3] with the 'medium' input to obtain individual ancillary response files (ARFS) and redistribution matrix files (RMFS). 'XISRESP' calls the tools 'XISRMFGEN' and 'XISSIMARFGEN'. Finally, we combined the spectra and response files from the two FI instruments (XIS0 and XIS3) using the FTOOL ADDASCASPEC. This procedure was repeated for each observation resulting in a total of four XIS spectra. The FTOOL GRPPHA was used to give at least 500 counts per spectral bin in every *Suzaku* observation mentioned in this paper. The hard X-ray detector (HXD) observations of Cyg X-1 will not be used in this work. The FI–XIS spectra were fitted in the 0.7–10.0 keV energy range. The results obtained with the BI spectra are not presented in this work as it is not expected to be different to that of the FI. In all fits to *Suzaku* data presented in this paper, the 1.9–2.5 keV energy range was ignored due to the possible presence of unmodelled instrumental features.

2.4 SWIFT J1753.5−0127

Using multiwavelength observations, Cadolle Bel et al. (2007) estimated the distance to SWIFT J1753.5−0127 (hereafter J1753) to be in the range of 4–8 kpc. This was based on the derived hydrogen column density along the line of sight to the source and its known latitude. From estimated bolometric flux and the assumption that

---

[1] If the accretion disc is ionized solely due to the hard X-rays from magnetic flares then a high-energy break is expected at the thermal temperature of the flares. However, it is possible that the source of hard radiation contains a hybrid of thermal/non-thermal electrons at which point a break is no longer necessary in the hard spectra.

[2] http://heasarc.gsfc.nasa.gov/docs/suzaku/analysis/

[3] http://suzaku.gsfc.nasa.gov/docs/suzaku/analysis/xisresp

the source is radiating at less than 5 per cent the Eddington luminosity, the authors constrained the mass of J1753 to approximately 4–16 M$_\odot$. This range is in agreement with the value of 12 M$_\odot$ estimated by Zurita et al. (2008) based on the orbital period of J1753. In the same work, Zurita et al. estimated a lower limit for the distance of 7.2 kpc. For the purpose of our work, we will assume a conservative range of 4–16 M$_\odot$ and 7.2–10 kpc for the mass and distance, respectively. The inner disc inclination was found from the reflection features in the *XMM–Newton* X-ray spectrum to be $55^{+2\circ}_{-7}$ (Reis et al. 2009).

Using *RXTE* and *XMM–Newton* data, Miller, Homan & Miniutti (2006) showed the presence of a cool (kT $\approx$ 0.2 keV) accretion disc extending close to the ISCO in the low-hard state of J1753. The presence of this cool accretion disc was later confirmed with *RXTE* observations during its 2005 outburst (Ramadevi & Seetha 2007). Reis et al. (2009b) have recently re-analysed the *XMM–Newton* and *RXTE* spectra of J1753 in the low-hard state and found that the disc likely extends to $r_{in} = 3.1^{+0.7}_{-0.6}\,r_g$. This strong constraint was based on the self-consistent modelling of both the reflection features and the soft thermal-disc component. An alternative interpretation was given by Hiemstra et al. (2009), however see 'note added after submission' in Reis et al. (2009b). In this work, we further explore the spectra described in Reis et al. (2009b) in the 0.5–10.0 keV energy range.

2.5 GRO J1655−40

GRO J1655−40 (hereafter J1655) has a compact object with a mass constrained to 6.3 $\pm$ 0.5 M$_\odot$ and orbital inclination of 70°.2 $\pm$ 1°.9 (Greene, Bailyn & Orosz 2001). Using radio observations, Hjellming & Rupen (1995) found a distance of 3.2 $\pm$ 0.2 kpc and an inner disc inclination of 85° $\pm$ 2°. In this work, we use an inclination of 70°.2 with a lower and upper limit of 68°.3 and 87°, respectively.

Using archival *ASCA* data of J1655 in outburst, Miller et al. (2005) showed evidence of a highly skewed, relativistic line, and suggested an inner accretion disc radius of $\approx 1.4 r_g$, indicative of a rapidly spinning black hole. This was later confirmed by Díaz Trigo et al. (2007) using simultaneous *XMM–Newton* and INTEGRAL observations of J1655 during the 2005 outburst. Brocksopp et al. (2006) followed the spectral evolution during the 2005 outburst using the *Swift* X-ray Telescope. They note the presence of a strong iron line at ≈ 6.4 keV in the single observation of the low-hard state;[4] however, they find no evidence of a thermal component. It is interesting that the neutral hydrogen column density (N_H) remains at an average of $\approx 6.9 \times 10^{21}$ cm^{-2} for all observations reported by Brocksopp et al. other than the single low-hard state observation where the value of N_H drops to $\approx 5.9 \times 10^{21}$ cm^{-2} (see their tables 4 and 5). It is plausible that a lower value of N_H can act to mask the presence of a weak soft component when the signal-to-noise ratio level is low (see Section 3).

Takahashi et al. (2008) have recently reported on the *Suzaku* observation of J1655 in the low-hard state where they find strong evidence for both a broad iron line and a soft disc component with a temperature of ≈ 0.2 keV. *Suzaku* observed J1655 on 2005 September 22, 07:32 UT for approximately 35 ks (Obs ID 100029010). The XISs were operated in the 3 $\times$ 3 and 2 $\times$ 2 editing mode with the '1/8 window' employed. XIS0 was not operational during the ob-

servation. The data were reduced in the standard way as described above for Cyg X-1. Source events were extracted from a circular region 70 pixels in radius centred on the source. The background is taken from a source-free region 50 pixels in radius towards the edge of the chip. The HXD was operated in its normal mode. The appropriate response and background files for XIS-nominal pointing were downloaded[5] and the HXD/PIN data were reprocessed in accordance with the Suzaku Data Reduction Guide. The XIS and PIN data were fitted in the 0.7–9.0 and 12.0–70.0 keV energy range, respectively. A normalization constant of 1.16 was applied to the PIN data in accordance with the latest *Suzaku* calibration report.

2.6 XTE J1118+480

Dynamical measurements of XTE J1118+480 (hereafter J1118) have set a strong constraint on the mass function of 6.1 $\pm$ 0.3 M$_\odot$ (McClintock et al. 2001; Wagner et al. 2001). Frontera et al. (2001) suggest that the black hole in J1118 has a mass of 7–10 M$_\odot$ with an orbital inclination in the range of 60°–80°. A recent study by Gelino et al. (2006) places a more stringent constraint of 8.53 $\pm$ 0.60 M$_\odot$ and 68° $\pm$ 2° for the mass and inclination, respectively. The authors find a distance of 1.72 $\pm$ 0.1 kpc to the system. To our knowledge, the broadest constraint on the distance to J1118 was that imposed by McClintock et al. (2001) of 1.8 $\pm$ 0.6 kpc. Since this range encompasses all the latest predictions, we employ this value in the work that follows. The inclination and mass are hereafter assumed to lie in the range 60°–83°[6] and 7–10 M$_\odot$, respectively.

J1118 was observed in its low-hard state by *Chandra*, *RXTE*, the United Kingdom Infrared Telescope, the *Extreme Ultraviolet Explorer* and the *Hubble Space Telescope* in 2000 as part of a multiwavelength, multi-epoch observing campaign. Based on these observation, McClintock et al. (2001) reported an apparent cool thermal component at ≈ 24 eV which was interpreted as originating in an accretion disc truncated at a radius greater than $70 r_g$. Reis, Miller & Fabian (2009) have recently re-analysed the *Chandra* and *RXTE* data and shown that the accretion disc is consistent with extending close to the ISCO, contrary to previous results. The *Chandra* and *RXTE* spectrum of J1118 in the low-hard state, as described in Reis, Miller & Fabian (2009), is used in the analyses that follows.

2.7 IGR J17497−2821

Unfortunately, very little is known about the properties of the newly discovered X-ray binary IGR J17497−2821 (hereafter J17497). Paizis et al. (2007) have placed the source in the direction of the Galactic Centre and argue that it must be either very close to or beyond the Galactic Centre. We assume the distance to J17497 to lie in the range 5–10 kpc. We are not aware of any estimates for the mass or inclination which we assume to be in the range 5–20 M$_\odot$ and 10°–80°, respectively. Paizis et al. (2008) presented the broadband *Suzaku* observation of J17497 in its low-hard state. They find that the data are best modelled with the sum of a thermal-disc component plus Comptonization. The accretion disc is found to have an inner temperature of ≈ 0.25 keV and a radius of ≈ 123 km for an assumed distance of 8 kpc and inclination of 60°. For a 10 solar mass black hole, the authors estimate that the disc extends to $\approx 11 r_g$ after correction for Compton upscattering.

---

[4]Brocksopp et al. (2006) analysed 20 *Swift* pointings covering the evolution from the low-hard, high-soft and very high state; however, only one pointing captured the source in the low-hard state.

[5]http://www.astro.isas.ac.jp/suzaku/analysis/hxd/
[6]The high value reflects the upper limit predicted by Wagner et al. (2001).

We analyse the 2006 September 25 observation (Obs ID 901003010). The XIS was operated in the 2×2 and 3×3 editing mode with the '1/4' window employed due to the brightness of the source. The data were reduced in the standard way as described above for Cyg X-1. Source events were extracted from a circular region 110 pixels in radius centred on the source. The background is taken from a source-free region 110 pixels in radius towards the edge of the chip. HXD data are not used in this analysis. Following Paizis et al. (2008), we do not use XIS data below 1 keV and limit the upper energy to 9 keV.

2.8 J1817−330

We are not aware of any constraints on the physical parameters of the newly discovered X-ray binary XTE J1817−330 (hereafter J1817; Remillard et al. 2006). For this reason, we assume the distance, mass and inclination to be in the range 1–15 kpc, 4–15 $M_\odot$ and $10°$–$80°$, respectively.

The *XMM–Newton* and *INTEGRAL* observations of the source in the soft state have been reported by Sala et al. (2007). The authors find that the data can be successfully modelled with the presence of a disc component with a temperature varying from approximately 1.0 to 0.7 keV and an inner radius of ≈ 50 km, assuming a distance of 10 kpc and $45°$ inclination. The source was later tracked through the decline of its outburst by the *Swift* satellite. Rykoff et al. (2007; hereafter R07) reported on the 21 snapshot observations tracking J1817 from the high-soft to the low-hard state. They found that the source follows closely the $L_X \propto T^4$ relation during the decline and argued that the accretion disc does not recede after the state transition down to accretion rates as low as $0.001 L_{\rm Edd}$. This work was later challenged by Gierlinski, Done & Page (2008) who, using the same *Swift* data as R07, argued that irradiation into the disc gives radii which are consistent with disc truncation.

Here, we re-analyse the data presented in R07 using the same reduction procedures detailed by the authors. Out of the 22 observations (see table 1 of R07) 13 are in the soft state, two are in the intermediate state and the latter six observations are in the low-hard state as described in Gierlinski et al. (2008). In this work, we will use observations 17–18 since the data quality in the latter observations of the low-hard state does not strongly require the presence of a disc. Following R07, observations 17 and 18 (hereafter Obs 1 and 2) were fitted in the 0.6–10.0 and 0.3–10.0 keV, respectively, with the absorbing column density fixed at 1.2×10^{21} cm^{-2}. We note

that the neutral hydrogen column density in the line of sight to the source is not thought to vary between observations (Miller, Cackett & Reis 2009). Table 1 summarizes the range in the various physical parameters used throughout this work.

3 ANALYSIS AND RESULTS

The X-ray spectrum (0.1–100 keV) of stellar mass BHBs in the low-hard state above a few keV is usually thought to be dominated by inverse Compton scattering of the soft thermal-disc photons in a cloud of hot electrons or 'corona' (Zdziarski & Gierlinski 2004). The geometry of the Comptonization region is still not firmly established. Certain models have hot electrons confined in magnetic flares above the cool accretion disc (Beloborodov 1999; Merloni, Di Matteo & Fabian 2000; Merloni & Fabian 2001) whilst others predict that the hard X-ray emission originates in the base of a jet (Markoff & Nowak 2004; Markoff et al. 2005). A further possibility is that the accretion flow consists of a thin disc truncated at large distances from the black hole ($R_{\rm tr} \gtrsim 10^3 r_{\rm g}$; Esin et al. 1997) and the hard emission originates in the hot, quasi-spherical advection-dominated accretion region close to the central source. In all these cases, the X-ray continuum in the $\sim$2–10 keV energy range can be phenomenologically modelled by a simple power law with a photon index between approximately 1.4 and 2, with major differences between the models arising at energies greater than $\sim$30 and below $\sim$2 keV.

We begin our analyses by fitting the various spectra up to a maximum energy of 10 keV with a power law modified by absorption in the interstellar medium (PHABS model in XSPEC). The equivalent neutral hydrogen column density ($N_{\rm H}$) is initially a free parameter in all observations. It is clear from Table 2 and Fig. 1 that the model is a poor description of the data to the majority of the objects. Strong curvature below $\sim$2 keV is clearly seen in all sources other than J17497 and J1817 possibly due to the poorer low-energy coverage in those observations. The excess and curvature seen at soft energies is characteristic of a thermal-disc emission and *cannot* be properly modelled by variation in the absorbing column density. This is a consequence of the high-quality data presented here. As an example of the way artificial variation in the absorbing column density can act to mask out the presence of a disc component, we constrain the value of $N_{\rm H}$ for Cyg X-1 to 5–9 $\times 10^{21}$ cm^{-2}; this covers the largest published range of $N_{\rm H}$ for this object (Dotani et al. 1997; Takahashi, Inoue & Dotani 2001; Miller et al. 2002; Torres et al.

Table 1. Summary of the various BHB physical parameters.

Source	Inclination (°)	Distance (kpc)	Mass ($M_\odot$)	Total flux[ab]	Disc flux[ab]
GX 339−4	10–30	6–10	10–20	16.6 ± 0.1	$2.20^{+0.09}_{-0.08}$
J1650−500	47–70	1.9–3.3	5.3–11.3	213.0 ± 2	61.2 ± 1.2
Cyg X-1 (1)	25–50	2.0–2.2	7–25	$133.1^{+3.7}_{-3.5}$	$23.7^{+3.2}_{-3.0}$
Cyg X-1 (2)	25–50	2.0–2.2	7–25	$109.6^{+3.7}_{-3.5}$	$15.5^{+3.2}_{-3.0}$
J1753.5−0127	49–57	7.2–10.0	4–16	4.10 ± 0.01	0.13 ± 0.01
J1655−40	68.3–87	3.0–3.4	5.8–6.8	9.5 ± 0.2	0.8 ± 0.2
J1118+480	60–83	1.2–2.4	7–10	13.0 ± 0.1	1.11 ± 0.05
J17497−2821	10–80	5–10	5–20	$15.6^{+1.7}_{-1.4}$	$6.2^{+1.7}_{-1.4}$
J1817−330 (1)	10–80	1–15	4–15	7.15 ± 0.15	$2.95^{+0.25}_{-0.27}$
J1817−330 (2)	10–80	1–15	4–15	$1.16^{+0.08}_{-0.07}$	0.19 ± 0.06

Note. Physical parameters for the various BHBs treated in this work. For references and explanations on the range quoted above please see Section 2. [a]Unabsorbed flux in units of $\times 10^{-10}$ erg cm^{-2} s^{-1} in the 0.5–10 keV energy range obtained using the XSPEC model CFLUX convolved with the model shown in Table 3. [b]The quoted errors for the fluxes are at the 90 per cent confidence.

Table 2. Results of fits to simple absorbed power-law model.

Source	N_H ($\times 10^{22}$ cm^{-2})	Γ	N_{PL} [c]	χ^2/ν
GX 339−4	0.420 ± 0.002	1.800 ± 0.004	0.256 ± 0.001	6723.5/1635
J1650−500	0.549 ± 0.002	2.562 ± 0.006	6.12 ± 0.03	7937.3/1275
Cyg X-1 (1)	0.339 ± 0.003	1.685 ± 0.005	1.66 ± 0.01	1088.9/724
Cyg X-1 (2)	0.346 ± 0.004	1.669 ± 0.006	1.41 ± 0.01	831.7/685
J1753.5−0127	0.175 ± 0.001	1.666 ± 0.003	0.0617 ± 0.0002	3044.6/1499
J1655−40	0.525 ± 0.003	1.660 ± 0.005	0.129 ± 0.001	1733.1/1441
J1118+480 [a]	$0.0080^{+0.0001}$	1.877 ± 0.005	0.222 ± 0.001	5451.8/4248
J17497−2821	4.349 ± 0.003	1.50 ± 0.01	0.114 ± 0.002	1246.6/1184
J1817−330 [b] (1)	0.12(f)	3.01 ± 0.04	0.215 ± 0.004	403.6/209
J1817−330 [b] (2)	0.12(f)	2.01 ± 0.07	0.0206 ± 0.0001	107.7/81

Note. [a] A lower limit on the absorbing column density of 8×10^{19} cm^{-2} is imposed. [b] For J1817 N_H is frozen at the value indicated. [c] The power-law normalization is referred as N and is given in units of photons keV^{-1} cm^{-2} s^{-1} at 1 keV. All errors refer to the 90 per cent confidence range for one parameter of interest.

2005; Makishima et al. 2008). Fitting the spectra with a power law now results in a much more distinct soft excess as can be seen in Fig. 2. A change in N_H from $\approx 3.4 \times 10^{21}$ cm^{-2} (Table 2) to 5×10^{21} cm^{-2} results in a dramatic difference to the modelled spectra of Cyg X-1 in the low-hard state. A similar behaviour is seen in J1118 where N_H peaks at the lower limit imposed of 8×10^{19} cm^{-2}. This behaviour has been reported for Cyg X-1 by Takahashi et al. (2001) using *ASCA* data and possibly explains the lower value of N_H found in the single *Swift* pointing of J1655 in the low-hard state (see tables 4 and 5 in Brocksopp et al. 2006).

Evidence of reflection features in the form of an excess at approximately 4–7 keV can be seen in all spectra other than J1118, J17497 and J1817. In the work that follows, we will ignore the 4–7 keV range in GX 339−4 and J1650 and the 5–7 keV range in Cyg X-1, J1753 and J1655. The reflection features will be individually explored in Section 3.5. Table 2 details the parameters obtained when fitting the various spectra with a simple absorbed power law. Although none of the fits is statistically acceptable, we show the results obtained with this model to emphasize the necessity of a further disc component in the spectra of BHBs in the low-hard state.

3.1 The requirement for a MCD component

The most widely used multicolour disc (MCD) model for the study of black holes accretion is the DISKBB model (Mitsuda et al. 1984). This simple model describes the spectrum from a geometrically thin and optically thick (Shakura & Sunyaev 1973) accretion disc consisting of multiple blackbody components. It is parametrized by the colour temperature and a normalization factor defined as $(r/d)^2 \cos\theta$, where r is the inner radius of the accretion disc in km, d is the distance to the source in units of 10 kpc and θ is the disc inclination. Table 3 details the parameters obtained when DISKBB is used to model the soft disc emission in the various sources. The addition of this model is required at greater than the 5σ level in *all* observations established using the FTEST command in XSPEC. The low temperature found in all sources would render the strong detection of the disc component impossible with *RXTE*.

The MCD model DISKBB assumes a non-zero torque boundary condition at the inner edge of the accretion disc (Gierlinski et al. 1999). This is contrary to the standard idea where the accretion disc extends down to an inner radius r_{in} at which point the material free falls rapidly with negligible viscous interaction. In order to test the effect of zero-torque and non-zero torque boundary conditions,

Zimmerman et al. (2005) constructed the MCD model EZDISKBB implementing the zero-torque boundary condition. Similar to the DISKBB model, EZDISKBB has as a parameter the colour temperature as well as a normalization described as $(1/f)^4 (r/d)^2 \cos\theta$, where we remind the reader that the colour correction factor, f, is the ratio between the colour temperature and the blackbody temperature of the disc, and all other symbols are similar to that of DISKBB.

To confirm that the results presented above do not depend on the choice of MCD model used, we have re-analysed the data with the model EZDISKBB. In what follows, we assume the standard value of 1.7 for the colour correction factor (Shimura & Takahara 1995) and set a lower and upper limit of 1.3 and 2, respectively, when calculating errors on the derived inner radius (see Section 3.4). Table 4 shows the results of the fits with the DISKBB model replaced by the zero-torque model EZDISKBB. Statistically we find no difference in the models between most of the fits, with the two models also giving very similar colour temperatures. We note here that all sources in our sample strongly require the presence of a thermal component. The question we will address below is whether this thermal emission arises from a small region extending close to the ISCO or from a larger, cooler region truncated far from the black hole.

3.2 Inner radius from the thermal component

The observed thermal-disc flux depends on the emitting area ($\propto r_{in}^2$), inclination and distance to the source. These are parametrized in the normalization of the DISKBB and EZDISKBB component as described above. Using the constraints on the physical parameters of the various sources along with the measured normalizations, we derived constraints on the innermost radius of the disc for the various sources. The derived values for the inner radius of the various sources in units of gravitational radii are shown in Tables 3 and 4.

Fig. 3 shows the derived inner radii from the normalizations of the DISKBB (top panel) and EZDISKBB (bottom panel) model as a function of the total unabsorbed luminosity. The inner radii obtained from the DISKBB model are shown as a function of disc luminosity in Fig. 4. The 3σ errors on the inner radii and luminosities shown in Figs 3–6 were estimated using Monte Carlo simulations. A uniform distribution was assumed for the masses, distances and inclinations of the various sources with the range shown in Table 1. The normalization of the MCD components and the fluxes were assumed to have a Gaussian distribution. When constraints, however mild, on the inclinations, masses and distances are available, we see from Figs 3 and 4 that the derived inner radii from the thermal continuum
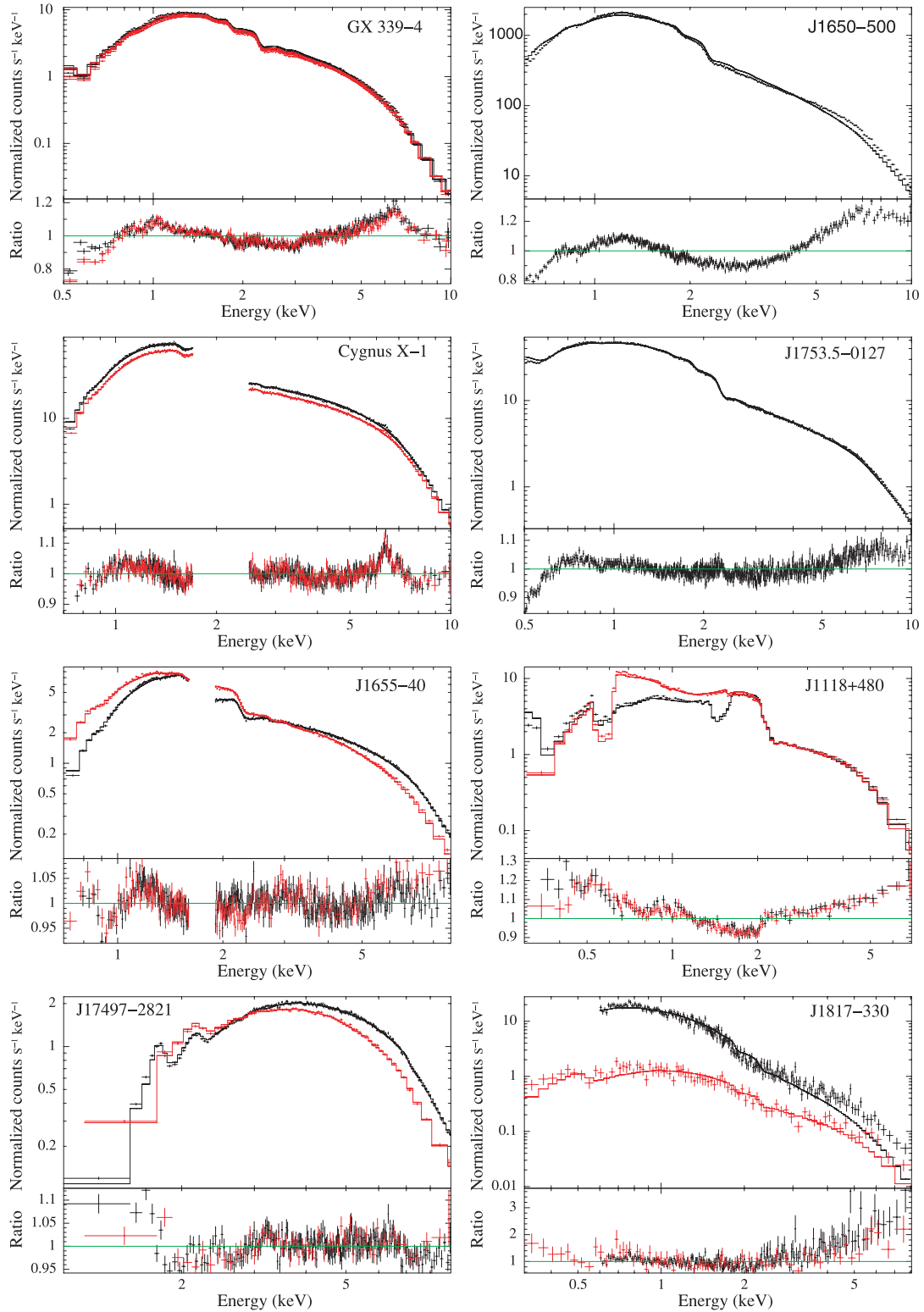
Figure 1. Data/model ratio to an absorbed power law. A simple power law does not provide a satisfactory model to any of the sources above. The excess and curvature below ≈ 2 keV is indicative of a thermal-disc component which is required at over 5σ level in all sources (see Section 3.1). GX339$-$4: EPIC–MOS1 and 2 data are shown in black and red respectively. Cyg X-1: Obs 1 and 2 are shown in black and red, respectively. J1655$-$40 and J17497$-$2821: FI and BI spectrum are shown in black and red, respectively. J1118+480: plus and minus first-order spectrum are shown in black and red, respectively. J1817$-$330: Obs 1 and 2 are shown in black and red, respectively. All spectra have been rebinned for plotting purposes only.
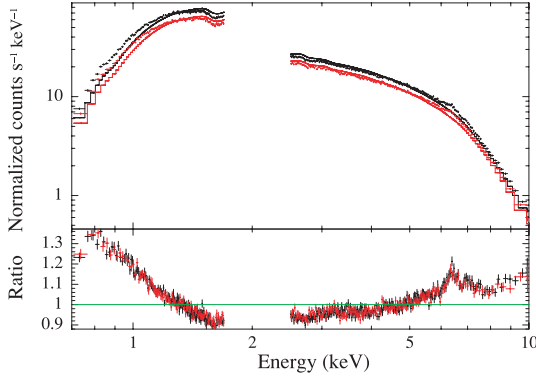
Figure 2. Ratio to power law for Cyg X-1 when the column density N_H is constrained to $5–8 \times 10^{21}$ cm^{-2} (see Section 3).

using the model DISKBB are below $\sim 10 r_g$ and *always* consistent with extending to the ISCO. In all cases other than the two sources with little constraints on the physical parameters (J17497 and J1817), the maximum value possible for the inner radius lies below $\sim 20 r_g$ at the 3σ confidence level. The results obtained from the EZDISKBB model (Fig. 3, bottom panel) are similar to that of DISKBB but for a factor of ≈ 1.34 higher. Figs 5 and 6 show the inner radii as a function of the Eddington ratio and colour temperature, respectively.

It can be seen from Figs 3 to 5 that the various BHBs investigated cover a wide range of both luminosities and Eddington ratios, with the least luminous source (J1118) being approximately two orders of magnitude less luminous than J1650. It is interesting to note from Fig. 5 that the majority of sources are clustered at $\sim 5–9 \times 10^{-3}$ L_{Edd} which is indicative of a mild selection effect in the sample.

3.3 Standard disc in the low-hard state

The standard Shakura–Sunyaev (SS) model predicts the accretion disc temperature to be $\sim (M/10 \, M_\odot)^{-1/4} (L/L_{Edd})^{1/4}$ keV (Shakura & Sunyaev 1973) for a disc extending to the ISCO. This gives a range in temperature of $\approx 0.15–0.35$ keV for the observed values of $L/L_{Edd} (\sim 5 \times 10^{-4}$ to 1.5×10^{-2}; Fig. 5). It can immediately be seen from Figs 6 and 7 that the range in temperature observed is in agreement with that predicted by the SS model given the values of the Eddington ratio found here. This shows that the behaviour of the accretion disc in the low-hard state for the various sources observed are characteristic of that predicted for a standard, geometrically thin disc. The results presented so far agree with that presented by R07 where the authors claim to see the presence of a standard accretion disc extending down to the ISCO until at 'least' $10^{-3} \, L_{Edd}$ in J1817.

3.4 Can a disc at $100 r_g$ radii explain the data?

In the previous section, we have shown using two well known MCD models that when the physical parameters of the systems are used

**Table 3.** Results of fits with the MCD component DISKBB and a power law.

Source	N_H ($\times 10^{22}$ cm^{-2})	Γ	N_{PL} [a]	kT (keV)	$N_{Diskbb} \times 10^3$	Inner radius[bc]	χ^2/ν
GX 339−4	0.495 ± 0.006	1.665 ± 0.009	$0.222^{+0.003}_{-0.0025}$	0.254 ± 0.006	$5.02^{+0.80}_{-0.67}$	$2.7^{+2.1}_{-1.2}$	2874.0/1633
J1650−500	0.556 ± 0.004	2.10 ± 0.01	3.40 ± 0.06	0.310 ± 0.004	55 ± 4	$7.3^{+7.1}_{-3.3}$	1507.9/1273
Cyg X-1 (1)	0.53 ± 0.02	1.71 ± 0.01	1.752 ± 0.025	$0.194^{+0.005}_{-0.004}$	236^{+63}_{-54}	$5.6^{+7.0}_{-3.0}$	783.1/722
Cyg X-1 (2)	0.50 ± 0.02	1.70 ± 0.01	1.485 ± 0.026	$0.194^{+0.007}_{-0.006}$	155^{+62}_{-49}	$4.6^{+6.3}_{-2.7}$	719.2/683
J1753.5−0127	0.197 ± 0.004	1.61 ± 0.01	0.0571 ± 0.0006	$0.274^{+0.015}_{-0.014}$	$0.32^{+0.11}_{-0.08}$	$1.5^{+2.3}_{-0.9}$	1961.0/1497
J1655−40	0.63 ± 0.02	1.67 ± 0.01	0.1333 ± 0.0019	0.21 ± 0.01	$5.4^{+2.7}_{-2.0}$	$5.9^{+6.8}_{-3.3}$	1618.8/1439
J1118+480	0.022 ± 0.003	1.69 ± 0.01	0.1864 ± 0.0028	0.21 ± 0.01	$7.4^{+1.4}_{-1.2}$	$2.3^{+2.6}_{-0.4}$	3747.3/4246
J17497−2821	4.72 ± 0.08	1.56 ± 0.01	$0.1282^{+0.0034}_{-0.0032}$	0.20 ± 0.01	54^{+49}_{-24}	14^{+40}_{-12}	1102.5/1182
J1817−330 (1)	0.12(f)	2.1 ± 0.1	$0.097^{+0.013}_{-0.012}$	0.20 ± 0.01	27^{+9}_{-6}	14^{+49}_{-13}	204.0/207
J1817−330 (2)	0.12(f)	1.5 ± 0.2	0.012 ± 0.003	0.21 ± 0.04	$1.3^{+1.5}_{-0.6}$	3^{+12}_{-3}	69.1/79

Note. Power-law normalization in units of keV^{-1} cm^{-2} s^{-1} at 1 keV. [b]The errors quoted for the various inner radii are the 3σ errors estimated using Monte Carlo simulations (see Section 3.2). [c]The inner radii are given in units of $r_g = GM/c^2$. All errors refer to the 90 per cent confidence range for one parameter of interest.

**Table 4.** Same as Table 3 but for the model containing EZDISKBB plus a power law.

| Source	N_H	Γ	N_{PL}	kT (keV)	$N_{Ezdiskbb} \times 10^3$	Inner radius	χ^2/ν
GX 339−4	$0.495^{+0.006}_{-0.005}$	$1.666^{+0.009}_{-0.008}$	$0.222^{+0.003}_{-0.002}$	0.241 ± 0.005	$1.1^{+0.2}_{-0.1}$	$3.5^{+4.4}_{-2.2}$	2885.5/1633
J1650−500	0.556 ± 0.004	2.10 ± 0.01	3.42 ± 0.06	0.293 ± 0.004	$12.0^{+0.9}_{-0.8}$	9^{+14}_{-6}	1509.1/1273
Cyg X-1 (1)	0.52 ± 0.02	1.71 ± 0.01	1.751 ± 0.025	$0.185^{+0.005}_{-0.004}$	49^{+13}_{-11}	7^{+13}_{-5}	782.4/722
Cyg X-1 (2)	0.50 ± 0.02	1.70 ± 0.01	1.484 ± 0.026	$0.185^{+0.007}_{-0.006}$	32^{+13}_{-10}	6^{+11}_{-4}	718.9/683
J1753.5−0127	0.197 ± 0.004	1.609 ± 0.007	0.0572 ± 0.0006	0.26 ± 0.01	0.075 ± 0.02	$2.0^{+4.1}_{-1.4}$	1969.2/1497
J1655−40	0.63 ± 0.02	1.67 ± 0.01	0.133 ± 0.002	0.20 ± 0.01	$1.1^{+0.6}_{-0.4}$	$7.4^{+12.0}_{-4.9}$	1618.9/1439
J1118+480	0.022 ± 0.003	1.69 ± 0.01	0.186 ± 0.003	0.20 ± 0.01	$1.6^{+0.3}_{-0.2}$	$3.0^{+4.6}_{-0.2}$	3746.0/4246
J17497−2821	4.72 ± 0.08	1.56 ± 0.01	0.128 ± 0.003	0.19 ± 0.02	$10.7^{+9.4}_{-4.7}$	17^{+57}_{-15}	1102.4/1182
J1817−330 (1)	0.12(f)	2.1 ± 0.1	$0.098^{+0.013}_{-0.012}$	0.19 ± 0.01	$5.9^{+1.9}_{-1.3}$	18^{+72}_{-17}	204.5/207
J1817−330 (2)	0.12(f)	1.5 ± 0.2	0.012 ± 0.003	$0.20^{+0.04}_{-0.03}$	$0.27^{+0.32}_{-0.13}$	4^{+17}_{-3}	69.1/79
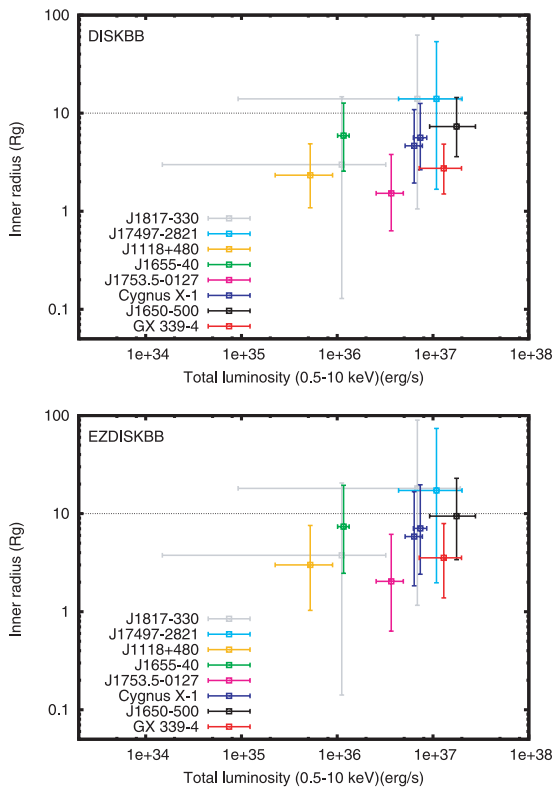
Figure 3. Inner radius versus total (unabsorbed) luminosity (0.5–10 keV). Top panel: r_{in} derived from the normalization of the DISKBB MCD model. Bottom panel: similar to above but for the EZDISKBB MCD model. The horizontal dashed line shows $r_{in} = 10 r_g$. The errors represent the 3σ confidence level estimated using Monte Carlo simulations (see Section 3.2).
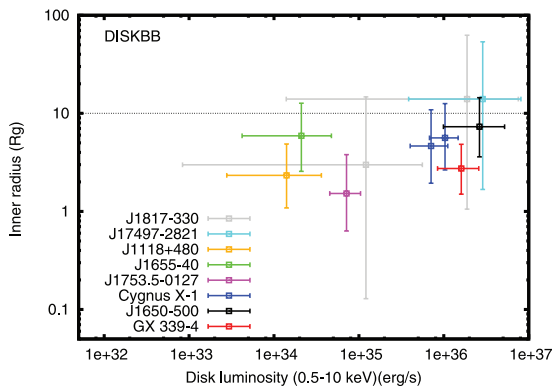
**Figure 4.** Inner radius versus disc luminosity (0.5–10 keV). The inner radius, r_{in}, is derived from the normalization of the DISKBB MCD model. The horizontal dashed line shows $r_{in} = 10 r_g$. All errors represent the 3σ confidence level.

in conjunction with continuum modelling, the accretion disc likely extends close to the ISCO in all sources investigated.

As previously mentioned, the ADAF model for accretion flow in the low-hard state has two distinct zones, with the inner part being modelled as a hot, optically thin advection-dominated region while the outer part consists of a standard SS disc. The transition radius is usually assumed to be $R_{tr} \sim O(10^3) r_g$ (Esin et al. 1997); however, Wilms et al. (1999) and Esin et al. (2001) have shown that for GX 339−4 and J1118 this radius is more likely to be 200–400r_g and $\approx 110 r_g$, respectively. In the work that follows, we will
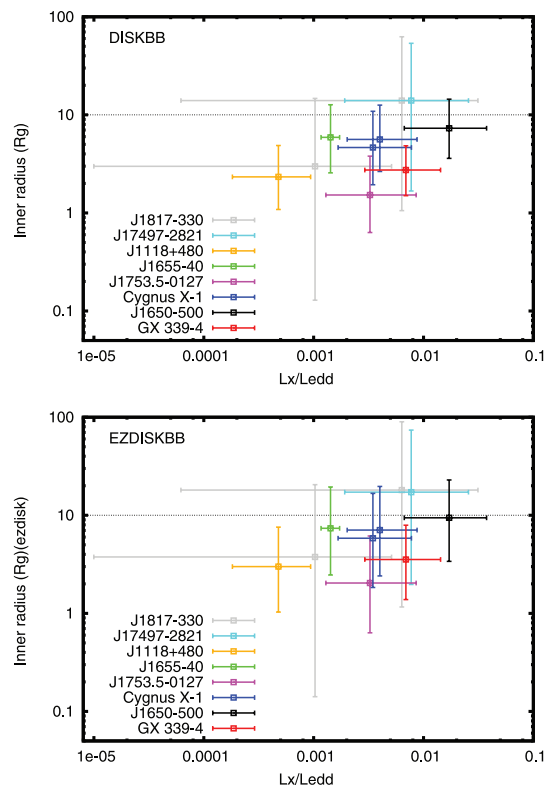
Figure 5. Inner radius versus L_X/L_{Edd}. Top panel: r_{in} from DISKBB. Bottom panel: r_{in} from EZDISKBB.
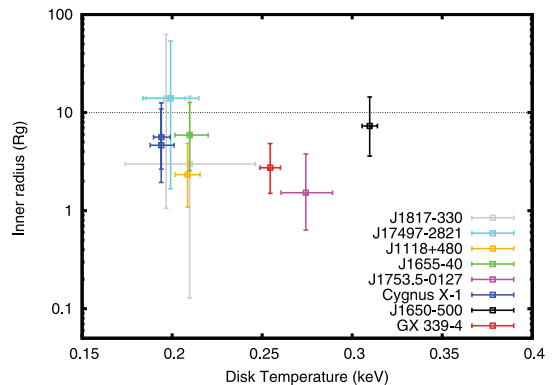

Figure 6. Inner radius obtained from the normalization of the DISKBB model versus disc temperature. The errors on the inner radii and disc temperature are 3σ and 1.64σ, respectively.

systematically investigate the possibility of having a disc truncated at $100 r_g$ in the sample of systems in the low-hard state presented here.

The model DISKPN (Gierlinski et al. 1999) is a further development of the DISKBB model taking into account the torque-free inner boundary condition.[7] This model has three parameters: the maximum colour temperature of the disc (T_{col}) in units of keV the inner disc radius, r_{in}, and the normalization which is defined as $m^2 \cos\theta/(D^2 f^4)$, where D is the distance to the source in kpc and all other symbols are similar to that of DISKBB and EZDISKBB. Given that

[7]It was in fact this work that pointed out the non-zero torque nature of the DISKBB model.
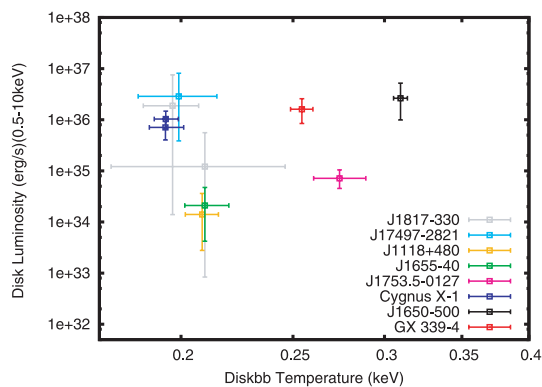
Figure 7. Disc luminosity as a function of disc temperature. Assuming a luminosity–temperature relation of $L_{\mathrm{disc}} \propto T_{\mathrm{BB}}^4$, we would expect to see a factor of 2–3 change in temperature for the range in luminosity shown in the plot. The errors on the luminosity and disc temperature are 3σ and 1.64σ, respectively.

the inner radius is now a parameter of the model, we perform fits where this value is fixed at both $6r_{\mathrm{g}}$ and $100r_{\mathrm{g}}$. As can be seen from Table 5, models with and without disc truncation give equally satisfactory fits. The temperature obtained in both cases is in remarkable agreement and only the normalization differs significantly.

The normalization of DISKPN, as well as of any other MCD model, conveys important physical information and can be used to set apart different, often contradictory, interpretations. Using the constraints on the masses and distances to the various sources (Table 1) together with the DISKPN normalizations for both $r_{\mathrm{in}} = 6$ and $100r_{\mathrm{g}}$, we plot the inclination as a function of the colour correction factor for each

source (Fig. 8). This factor is usually assumed to be a constant close to 1.7 for a wide range in luminosity (Shimura & Takahara 1995). Davis et al. (2005) showed that below a colour temperature of ~ 1 keV the colour correction factor is indeed a constant close to 1.7. Above this temperature, disc ionization leads to a slight increase in f; however, it is found to be consistently below ~ 2.2 (Davis, Done & Blaes 2006; Done & Davis 2008). Contrary to this, it was suggested by Merloni, Fabian & Ross (2000) that f is a relatively strong function of accretion rates varying from ≈ 1.7 to 3.

The solid red and green curves in (Fig. 8) show the dependence of the inclination on the colour correction factor for an accretion disc at 100 and $6r_{\mathrm{g}}$, respectively. The errors, shown by the shaded regions, are the 3σ errors estimated by Monte Carlo simulations assuming a uniform distribution of the mass and distance to the various sources (see Table 1) and the DISKPN normalization shown in Table 5. It can be seen that for most sources a disc truncated at $100r_{\mathrm{g}}$ requires a high colour correction factor which is, in most cases, inconsistent with the upper limit of three (solid vertical line) set by Merloni, Fabian & Ross (2000). We show in Section 4.1 that this value is in fact likely to be below ≈ 2.4 and the value of 3 used here is a conservative upper limit. J17497 and J1817 are the only sources where a truncated accretion disc is not ruled out due to the weak constraints on their masses, distances and inclinations. However, we have seen from the previous section that the data for these sources are suggestive of a disc extending to within $10r_{\mathrm{g}}$.

3.5 Inner radius from disc reflection

So far, we have only focused on the thermal component which in the low-hard state is predominant below ~ 2 keV. In the following

Table 5. Results for DISKPN fits with the inner radius fixed at $6r_{\mathrm{g}}$ (top) and $100r_{\mathrm{g}}$ (bottom). It can be seen that for most sources the parameters and statistics do not vary between models. The only exception to this is the large differences in the normalization of DISKPN. We can use this difference in conjunction with physical parameters (inclination, mass and distances; see Table 1) to differentiate between these two contradictory interpretations (see Section 3.4). All errors are quoted at the 90 per cent confidence level.

Source	N_{H}	Γ	N_{PL}	kT (keV)	N_6	χ^2/ν
GX 339$-$4	$0.496^{+0.006}_{-0.005}$	$1.666^{+0.009}_{-0.008}$	$0.222^{+0.003}_{-0.002}$	0.241 ± 0.005	0.09 ± 0.01	2887.6/1633
J1650$-$500	0.556 ± 0.004	2.10 ± 0.01	3.42 ± 0.06	0.293 ± 0.004	$1.03^{+0.08}_{-0.07}$	1508.9/1273
Cyg X-1 (1)	0.52 ± 0.02	1.71 ± 0.01	1.75 ± 0.02	$0.185^{+0.005}_{-0.004}$	$4.1^{+1.1}_{-0.9}$	782.5/722
Cyg X-1 (2)	0.50 ± 0.02	1.70 ± 0.01	1.48 ± 0.03	$0.185^{+0.007}_{-0.006}$	$2.71^{+1.1}_{-0.9}$	718.9/683
J1753.5$-$0127	$0.198^{+0.004}_{-0.005}$	$1.610^{+0.006}_{-0.008}$	$0.0573^{+0.0005}_{-0.0006}$	0.25 ± 0.01	0.006 ± 0.002	1970.4/1497
J1655$-$40	0.63 ± 0.02	1.67 ± 0.01	0.133 ± 0.002	0.20 ± 0.01	$0.096^{+0.047}_{-0.036}$	1618.9/1439
J1118$+$480	0.023 ± 0.003	1.69 ± 0.01	0.186 ± 0.003	$0.199^{+0.006}_{-0.007}$	$0.135^{+0.03}_{-0.02}$	3744.9/4246
J17497$-$2821	4.72 ± 0.08	1.56 ± 0.01	0.128 ± 0.003	0.191 ± 0.015	$0.9^{+0.8}_{-0.4}$	1102.4/1182
J1817$-$330 (1)	0.12(f)	2.1 ± 0.1	$0.098^{+0.013}_{-0.012}$	0.19 ± 0.01	$0.5^{+0.2}_{-0.1}$	204.5/207
J1817$-$330 (2)	0.12(f)	1.5 ± 0.2	0.012 ± 0.003	$0.20^{+0.04}_{-0.03}$	$0.02^{+0.03}_{-0.01}$	69.0/79

Source	N_{H}	Γ	N_{PL}	kT (keV)	N_{100}	χ^2/ν
GX 339$-$4	$0.499^{+0.004}_{-0.008}$	1.67 ± 0.01	$0.222^{+0.002}_{-0.003}$	$0.254^{+0.008}_{-0.004}$	$0.00215^{+0.0002}_{-0.0004}$	2880.4/1633
J1650$-$500	0.557 ± 0.004	2.10 ± 0.01	3.40 ± 0.06	0.311 ± 0.004	0.022 ± 0.002	1506.7/1273
Cyg X-1 (1)	0.53 ± 0.02	1.71 ± 0.01	1.75 ± 0.02	$0.195^{+0.005}_{-0.004}$	$0.10^{+0.03}_{-0.02}$	783.42/722
Cyg X-1 (2)	0.50 ± 0.02	1.70 ± 0.01	1.49 ± 0.03	$0.195^{+0.007}_{-0.006}$	$0.06^{+0.03}_{-0.02}$	719.5/683
J1753.5$-$0127	0.196 ± 0.002	1.61 ± 0.01	$0.0570^{+0.0007}_{-0.0004}$	$0.28^{0.01}_{-0.02}$	$0.00012^{+0.00005}_{-0.00002}$	1963.5/1497
J1655$-$40	0.63 ± 0.02	1.67 ± 0.01	0.133 ± 0.002	0.21 ± 0.01	0.002 ± 0.001	1618.6/1439
J1118$+$480	0.023 ± 0.003	1.69 ± 0.01	0.186 ± 0.003	0.210 ± 0.007	$0.0030^{+0.0006}_{-0.0005}$	3742.7/4246
J17497$-$2821	4.72 ± 0.08	1.56 ± 0.01	0.128 ± 0.003	0.20 ± 0.02	$0.02^{+0.02}_{-0.01}$	1102.5/1182
J1817$-$330 (1)	0.12(f)	2.1 ± 0.1	$0.097^{+0.013}_{-0.012}$	0.20 ± 0.01	$0.011^{+0.003}_{-0.002}$	203.6/207
J1817$-$330 (2)	0.12(f)	1.5 ± 0.2	0.012 ± 0.003	0.21 ± 0.04	$0.0005^{+0.0006}_{-0.0002}$	69.0/79
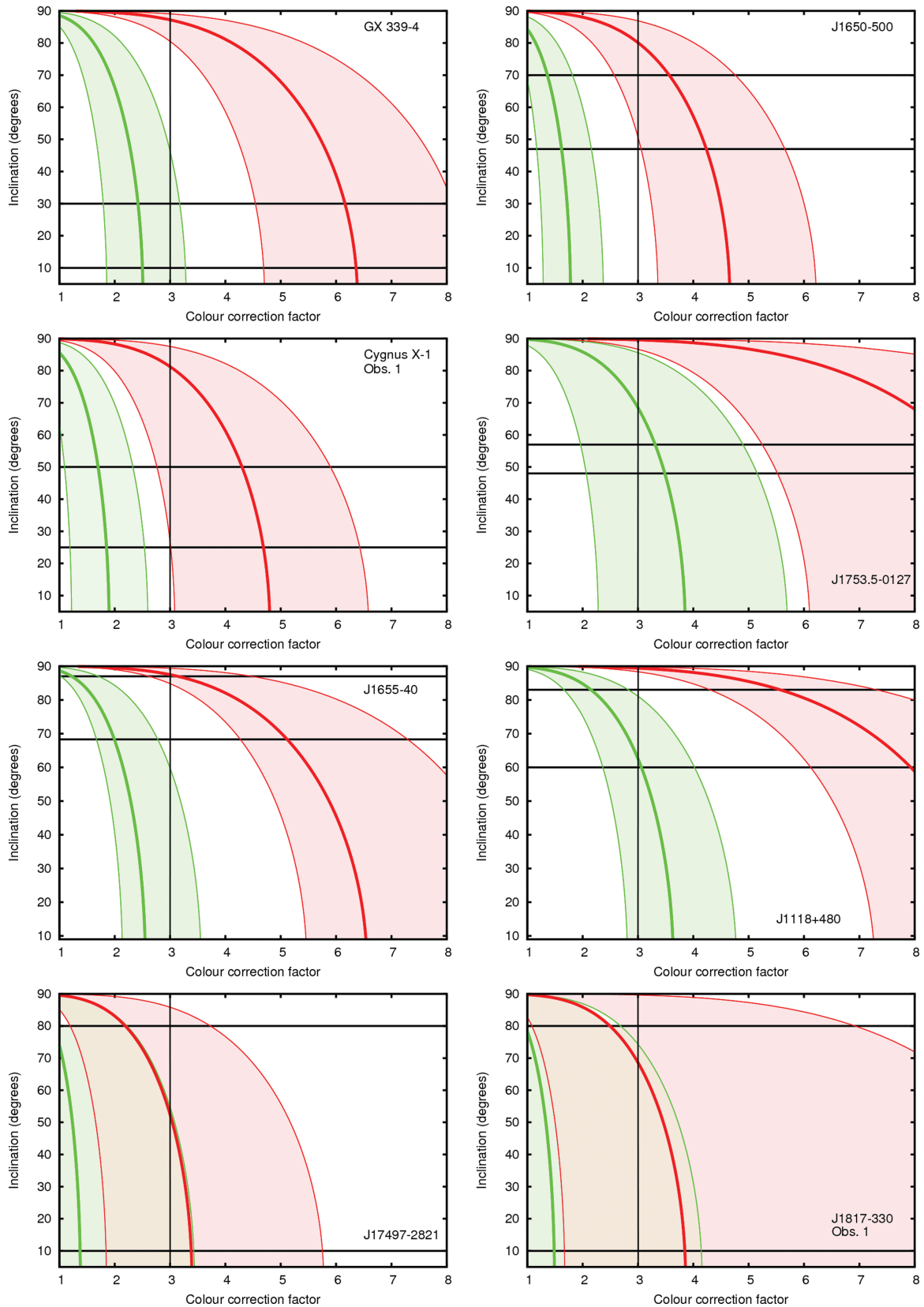
Figure 8. Inclination versus colour correction factor *f* for the various sources. The red and green curves are for a disc with inner radius of $100r_g$ and $6r_g$, respectively. The shaded regions shows the 3σ error range. The upper and lower limits on the inclination are given by the solid horizontal lines and the maximum expected colour correction factor is show by the solid vertical line. For the model to be physically consistent, the shaded region needs to be enclosed within the inclination range and to the left of the vertical line. This criteria rules out a disc at $100r_g$ for all sources other than J17497 and J1817. For simplicity, only the first observations of Cyg X-1 and J1817 are shown.

section, we will divert our attention to the reflection features present in five of the sources in our sample. To this end, we will ignore the energies below 3 keV in all spectra and, where possible, extend the high energy using either *RXTE* or *Suzaku* PIN data. A detailed analyses of each individual source is presented below.

3.5.1 J1650−500

We have initially added the *RXTE* PCA data up the 12 keV to the *XMM–Newton* spectrum in order to have a clearer view of the continuum. The absorbing column density was fixed at the value quoted in Table 3. An absorbed power law does not provide a satisfactory fit ($\chi^2/\nu = 1988.1/1411$), with the bulk of the residuals coming from the iron line region.

The standard and most generally used model for a relativistic line profile around a rotating black hole is the LAOR model in XSPEC (Laor 1991). It describes a broad line from an accretion disc surrounding a rotating Kerr black hole, with an emissivity profile described by a power law of the form $\epsilon_r = r^{-q}$. We use this model to account for the broad residuals seen at the iron line region. The LAOR model is calculated with the presumption of a maximally rotating black hole. Relativistic line models in which the black hole spin is a free parameter are now available (KYRLINE and KERRDISK models; Dovciak, Karas & Yaqoob 2004 and Brenneman & Reynolds 2006, respectively); however, we choose to use the well-established LAOR model as we are not interested in the precise value of the inner radius/spin and to allow for a more direct comparison with previous work. The outer disc radius in the LAOR model was fixed at the maximum allowed value of $400r_g$ and the inclination was constrained to the values shown in Table 1 (47°–70°) for J1650. The line energy was constrained to 6.4–6.97 keV. This resulted in a marked improvement over the previous fit with $\Delta\chi^2/\Delta\nu = -451.1/5$. A better fit is achieved when we allow the photon indices of the *XMM–Newton*

and *RXTE* observations to differ by ≤0.15. Miller (2009) has shown that small differences in the value of Γ between various X-ray instruments are expected and we allow such deviations in all combined *RXTE–XMM–Newton* analyses. The best fit ($\chi^2/\nu = 1352.2/1405$) in the 3–12 keV range is shown in Fig. 9 (top-left panel) and detailed in Table 6. Fig. 9 (top-right panel) shows a plot $\Delta\chi^2$ versus inner radius obtained with the command STEPPAR in XSPEC. Based on this analyses, the accretion disc in J1650 is found to be within $6r_g$ at more than the 5σ level of confidence (Fig. 9).

Fig. 9 (bottom panel) shows the best fit mentioned above extended to 100 keV after the addition of HXTE data. The power-law indices of both *RXTE* instruments are tied to each other. To make this figure, we have normalized the HXTE data so that the flux at 25 keV matches that of the PCA. The large excess peaking at ∼30 keV is the 'Compton hump' associated with reflection of hard X-rays by a cool accretion disc. In order to model the full spectra, we will use the reflection model REFLIONX (Ross & Fabian 2005) blurred with the same kernel used in the LAOR model (KDBLUR in XSPEC). The best REFLIONX fit covering the full energy band is shown in Fig. 10 (left-hand panel) and detailed in Table 7. When using the reflection model REFLIONX, the Fe Kα line, as well as the Compton hump, is modelled self-consistently. It should be noted that the refection component cannot account for the soft excess explored in the previous chapters in any of the sources investigated here. To emphasize this point, we show in Fig. 10 (right-hand panel) the data/model ratio of the best-fitting reflection model of J1650 extrapolated to the soft energy range. It is clear from this figure that a soft disc component is still required.

3.5.2 GX339−4

The presence of strong iron line emission in the *XMM–Newton* spectrum of GX 339−4 was previously seen in Fig. 1. A power-law
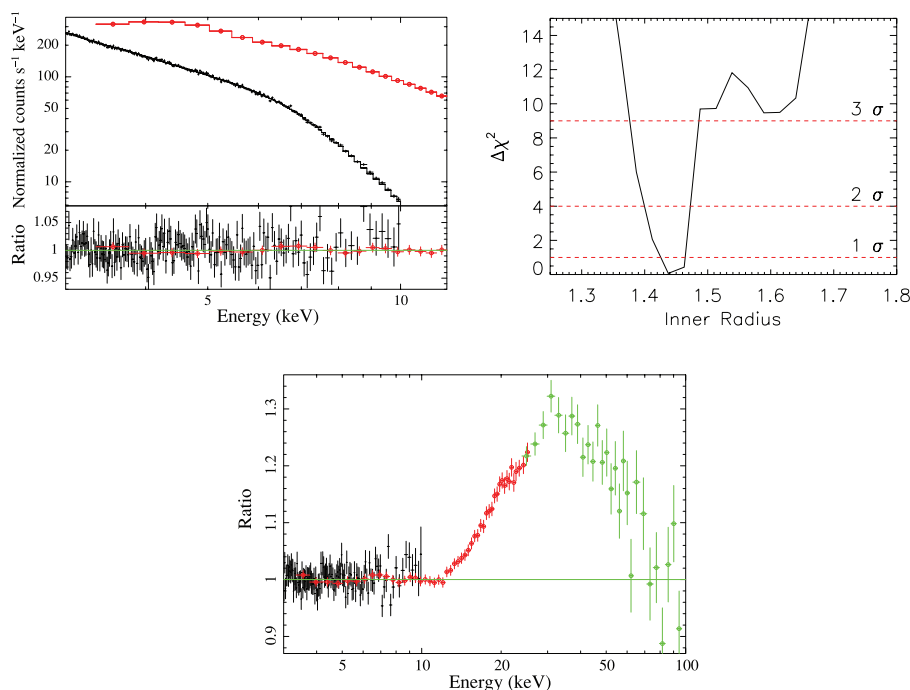
Figure 9. Top-left panel: best-fitting model for J1650−500 in the 3–12 keV energy range (Table 6). The *XMM–Newton* data are shown in black with *RXTE* PCA data shown in red. Top-right panel: goodness-of-fit variation as a function of inner radius. The horizontal lines mark the 1σ, 2σ and 3σ level. A disc radius greater than $6r_g$ is excluded at the 5σ level (not shown). Bottom panel: ratio of the best-fitting model above to the full, extended data. The HXTE (green) flux at 25 keV is normalized to match that of the PCA. The data have been rebinned for display purposes only.

Table 6. Results of fits with the LAOR line profile and a power law above 3 keV. GX 339−4 and J1650 were fitted in the 3–12 keV range. For J1655, we used *RXTE* up to 20 keV and J1753 covered the full 3–100 keV range. For Cyg X-1, only the XIS data were used up to 10 keV. The latter fit also included a narrow Gaussian line at 6.4 keV. The upper energy limits were chosen so as to exclude the prominent Compton hump present in most sources. The values of N_H are frozen at that shown in Table 3 and are given in units of 10^{21} cm^{-2}.

Parameter	N_H	Γ	N_{PL}	E_{LAOR} (keV)	q	θ (°)	r_{in} (r_g)	$N_{LAOR}(\times 10^{-3})$	χ^2/ν
J1650−500	0.556	2.17 ± 0.01	$3.70^{+0.07}_{-0.01}$	$6.97_{-0.09}$	$7.8^{+0.5}_{-0.4}$	65^{+5}_{-1}	$1.45^{+0.03}_{-0.04}$	37^{+3}_{-2}	1352.2/1405
GX 339−4	0.495	$1.671^{+0.012}_{-0.005}$	$0.225^{+0.004}_{-0.003}$	$6.93^{+0.04}_{-0.21}$	3.2 ± 0.5	10^{+17}	$2.4^{+0.3}_{-0.5}$	$3.6^{+0.3}_{-0.8}$	1906.4/1786
Cyg X-1 (1)	0.53	1.71 ± 0.01	1.75 ± 0.02	$6.97_{-0.04}$	$3.4^{+0.5}_{-0.3}$	20^{+4}	$6.3^{+1.4}_{-0.8}$	6.6 ± 1.0	647.9/636
Cyg X-1 (2)	0.50	1.70 ± 0.01	$1.48^{+0.02}_{-0.03}$	$6.97_{-0.08}$	$3.6^{+0.9}_{-0.6}$	20^{+3}	$7.1^{+2.3}_{-1.5}$	5.9 ± 1.0	561.3/549
J1753.5−0127	0.197	1.60 ± 0.01	0.056 ± 0.001	6.4(f)	$2.2^{+0.4}_{-0.3}$	67^{+8}_{-4}	$2.4^{+1.8}_{-1.2}$	0.14 ± 0.05	1450.8/1467
J1655−40	0.63	$1.74^{+0.1}_{-0.2}$	$0.144^{+0.003}_{-0.005}$	$6.47^{+0.07}_{-0.06}$	2.7 ± 0.3	86.0 ± 0.2	$1.5^{+0.2}_{-0.1}$	$2.3^{+0.2}_{-0.4}$	921.1/922
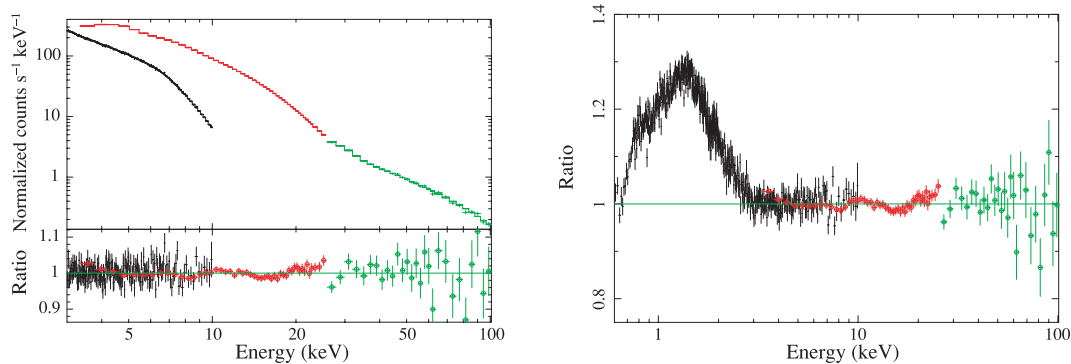
Figure 10. Left-hand panel: the best-fitting reflection model for J1650−500. Right-hand panel: ratio of the best-fitting reflection model to the 0.6–100.0 keV range. The strong soft excess clearly demonstrates the requirement for a further thermal-disc component.

Table 7. Results of fits to the full energy range using the reflection model REFLIONX. Both the Compton hump and the iron line profile are modelled self-consistently. The inner radius is found from the blurring of the reflection component. The values of N_H are frozen at that shown in Table 3 and are given in units of 10^{21} cm^{-2}.

Parameter	N_H	Γ	ξ(erg cm s^{-1})	q	r_{in} (r_g)	θ (°)	N_{PL}	$N_{REFLIONX}(\times 10^{-6})$	χ^2/ν
J1650−500	0.556	2.19 ± 0.02	620^{+130}_{-45}	$7.7^{+0.2}_{-0.3}$	1.3 ± 0.1	70_{-1}	$2.5^{+0.2}_{-0.1}$	102^{+11}_{-13}	1441.5/1461
GX 339−4	0.495	$1.72^{+0.01}_{-0.02}$	500^{+40}_{-90}	3.0 ± 0.1	2.1 ± 0.3	28^{+2}_{-18}	$0.188^{+0.004}_{-0.006}$	12^{+2}_{-3}	1935.6/1839
J1655−40	0.63	$1.71^{+0.01}_{-0.02}$	240^{+17}_{-15}	$2.72^{+0.7}_{-0.5}$	$1.38^{+0.6}_{-0.1}$	87_{-1}	$0.118^{+0.001}_{-0.003}$	12^{+2}_{-1}	957.7/966

fit over the 3–12 keV range results in a poor fit with $\chi^2/\nu = 2617.7/1791$. This is dramatically improved by the addition of the LAOR line model resulting in $\Delta\chi^2/\Delta\nu = -711.3/5$ with an inner radius approaching that expected for a maximally rotating black hole (Fig. 12).
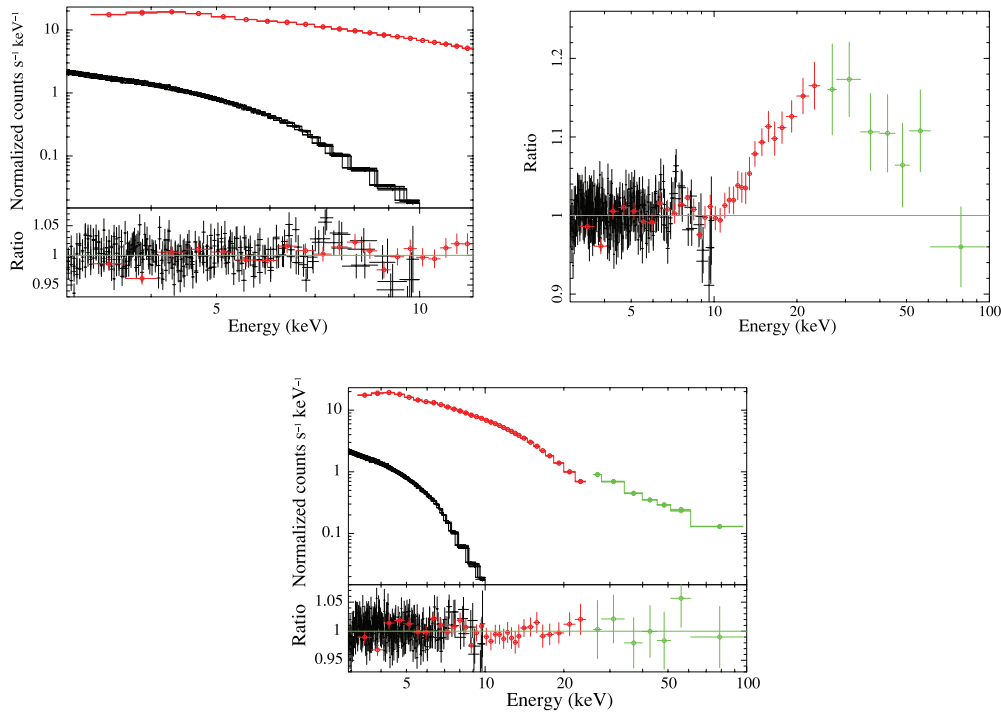
Fig. 11 (top-left panel) shows the best-fitting model over the 3–12 keV energy range. The fit extended to the full 3–100 keV range is shown in Fig. 11 (top-right panel) with the HXTE flux normalized to match that of the PCA at 25 keV. Similar to the spectra of J1650, this source shows the presence of a strong Compton reflection hump as expected from a source with strong fluorescence emission. Replacing the LAOR component with the blurred reflection model results in an acceptable fit to the full energy range (Fig. 11, bottom panel) with the inner radius again implying a maximally rotating black hole. Based on the extent of the gravitational blurring of the reflection features in GX 339−4, an accretion disc with an inner edge at a distance greater than $6r_g$ is excluded at more than the 5σ confidence level.

The value for the inner radius found using the full spectra ($2.0 \pm 0.3\,r_g$) is similar to that obtained in the narrower (3–12 keV) range

from the iron line shape alone ($2.4^{+0.4}_{-0.5}\,r_g$; Fig. 12). This emphasizes the robustness of spin measurements made from the shape of such strong reflection features. The result presented for the innermost extent of the accretion disc in the low-hard state is similar to that found for GX 339−4 in both the intermediate state ($2.0–2.2r_g$; Miller et al. 2008) and the joint fitting of the low-hard and very high state ($2.0–2.1r_g$; Reis et al. 2008) which confirms that the disc remains stable during these three spectral states.

3.5.3 Cygnus X-1

The profile around the iron Kα region in Cyg X-1 cannot be modelled with a single relativistic line (Fig. 13; left-hand panel). However, satisfactory fits are obtained for both observations by the addition of a narrow Gaussian at 6.4 keV together with the LAOR line. This resulted in $\chi^2/\nu = 647.9/636$ and $\chi^2/\nu = 561.3/552$ for Obs 1 and 2, respectively. The Gaussian is required at more than the 5σ level of confidence (*F*-value = 28.0 and probability = 1.7×10^{-7}). In both observations the inner radii and the emissivity indices are well constrained, and it can be seen from Fig. 14 that

Figure 11. Top-left panel: best-fitting model for GX 339−4 in the 3–12 keV energy range (Table 6). The *XMM–Newton* and *RXTE* PCA data are shown in black and red, respectively. Top-right panel: data/model ratio for the above model extended to 100 keV. The HXTE (green) flux at 25 keV is normalized to match that of the PCA (red). Bottom panel: best-fitting reflection model (Table 7).
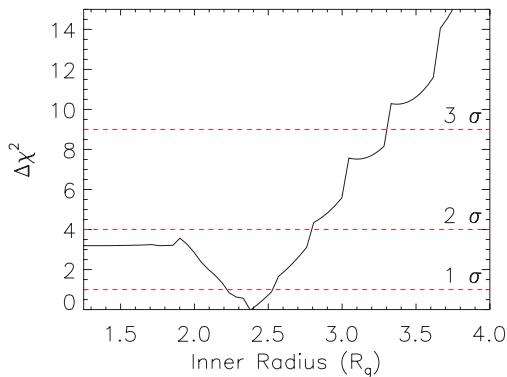
Figure 12. Goodness-of-fit variation as a function of inner radius for GX 339−4. The horizontal lines mark the 1σ, 2σ and 3σ level. A disc radius greater than $6r_g$ is excluded at the 5σ level (not shown).

the subtle correlation between these parameters does not provide a satisfactory solution with large radii for any physical values of emissivity. Table 6 details the various parameters in the model. The inner radii are constrained to $6.4^{+1.4}_{-1.0}$ and $7.1^{+2.3}_{-1.5} r_g$ (90 per cent confidence) in Obs 1 and 2 respectively, as shown in Fig. 15.

3.5.4 J1655−40 and J1753.5−0127

Fig. 16 shows the best-fitting model consisting of a power law and the LAOR line profile for both J1655 (left-hand panel) in the 3–20 keV energy range and J1753 (right-hand panel) in the full range. The relatively weak reflection features in J1753 does not allow for a strong constraint on the inner radius using simple phenomenological models, with a disc at greater than $20r_g$ only being ruled out at the 3σ level (Fig. 18; right-hand panel). However, Reis et al. (2009b)

showed using a self-consistent reflection model that when the full energy range (0.5–100.0 keV) is considered the value of the inner radius is constrained at approximately 2.5–$5.0r_g$ in agreement with the value found in Section 3.1 (Table 3). Extending the fit in J1655 to the full 3.0–70.0 keV range again shows the presence of a Compton hump (Fig. 17; left-hand panel) which is successfully modelled with the reflection model REFLIONX (Fig. 17; right-hand panel). The inner accretion disc radius in J1655 is constrained to less than $6r_g$ at more than 5σ confidence (Fig. 18; left-hand panel). Table 7 details the parameters found for the fit over the full energy range using REFLIONX.

In all sources investigated in this section, the equivalent widths of the Fe Kα line as modelled with the LAOR line profile have been found to be consistently above 70 eV at the 90 per cent confidence level. The only exception to this was J1753 where the equivalent width is found to be approximately 50 eV. In the following chapter, we consolidate our results and discuss the implication they have on models for accretion flow.

4 SUMMARY AND DISCUSSION

In this work, we have systematically analysed a sample of eight high-quality, stellar mass black hole spectra obtained with various CCD and grating instruments. We show observational evidence for the possible presence of an optically thick accretion disc extending close to the ISCO in all eight sources in the low-hard state. In half of the sources, the evidence comes from *both* the highly significant thermal component and blurred reflection features.

### 4.1 Constraints from the thermal disc

In all the objects studied, the presence of a low-energy soft excess is seen when the spectra are fitted with an absorbed power law (Fig. 1).
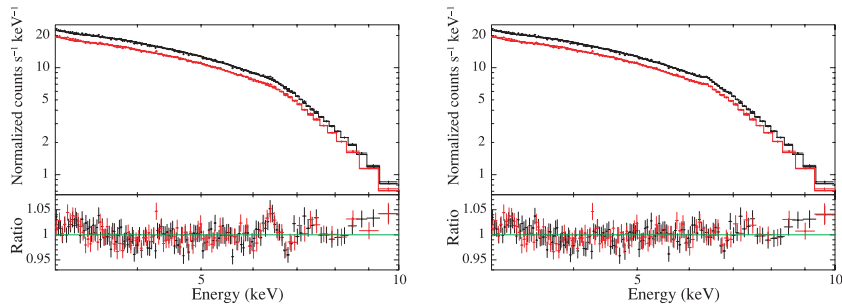
Figure 13. Left-hand panel: data/model ratio for Cyg X-1 with a power law and relativistic line. Right-hand panel: with the addition of a narrow Gaussian at 6.4 keV. Obs 1 and 2 are shown in black and red, respectively.
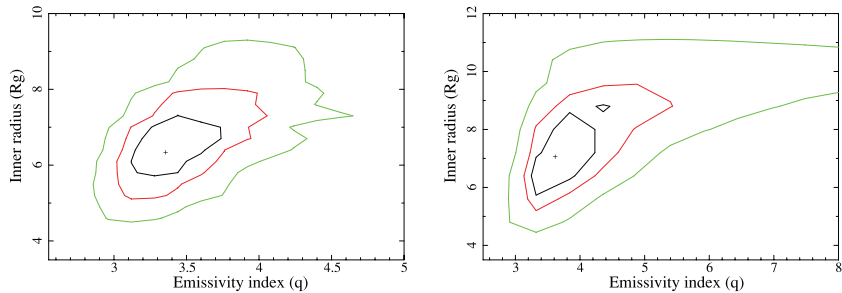
Figure 14. Emissivity versus inner radius contour plot for Cyg X-1. The 68, 90 and 95 per cent confidence range for two parameters of interest are shown in black, red and green, respectively. It can be seen that for the full range of the emissivity the inner radius is constrained between approximately $5-8r_g$ (Obs 1; left-hand panel) and $5-9r_g$ (Obs 2; right-hand panel) at the 90 per cent confidence level for two parameters.
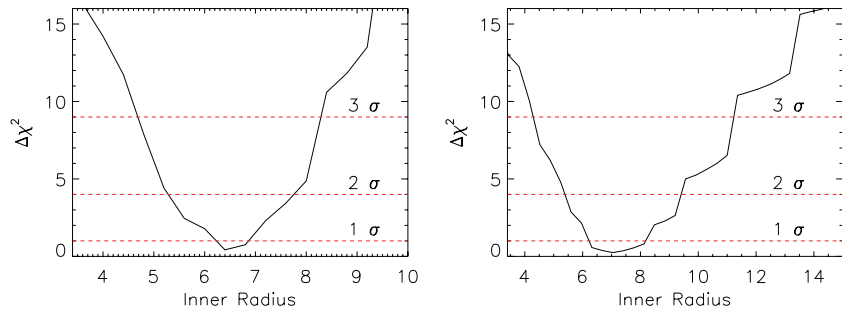

Figure 15. Left-hand panel: goodness-of-fit variation as a function of inner radius for Cyg X-1 (Obs 1). Right-hand panel: same but for Obs 2. The horizontal lines mark the 1σ, 2σ and 3σ level.
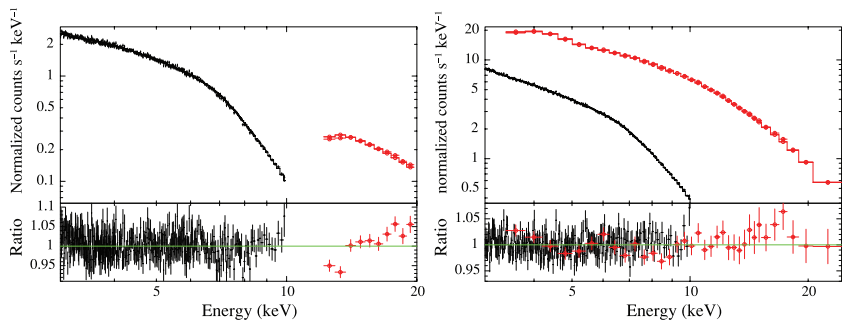

Figure 16. Best-fitting model consisting of power law plus relativistic line. Left-hand panel: J1655−40 in the 3–20 keV range. Right-hand panel: J1753.5−0127 in the 3–100 keV range. The HXTE data are omitted for display only.

This excess is traditionally modelled assuming thermal emission from an accretion disc where the flux, and hence normalization, is related to the disc inner radius according to $N \propto r_{in}^{2}$. In Sections 3.2 and 3.4, we have used this information along with constraints on the inclinations, masses and distances to the sources found in the literature to obtain the inner radius of accretion for the various sources. The results are shown in Figs 3–6. For six out of the eight sources investigated, the 3σ upper limit on their inner radii are
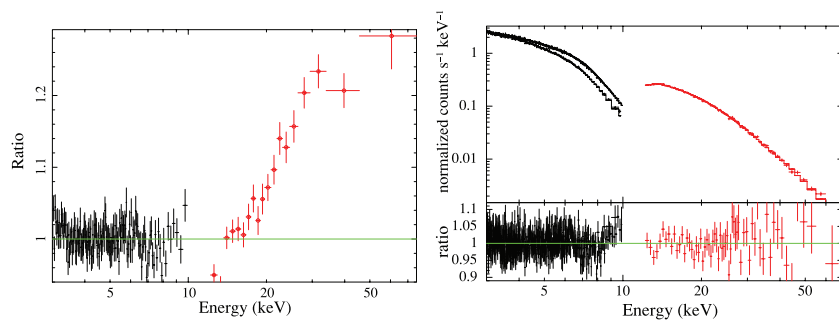
Figure 17. Left-hand panel: data/model ratio for J1655−40 with a model consisting of power law plus relativistic line fitted in the 3–20 keV range. Right-hand panel: best-fitting reflection model in the full 3–70 keV range.
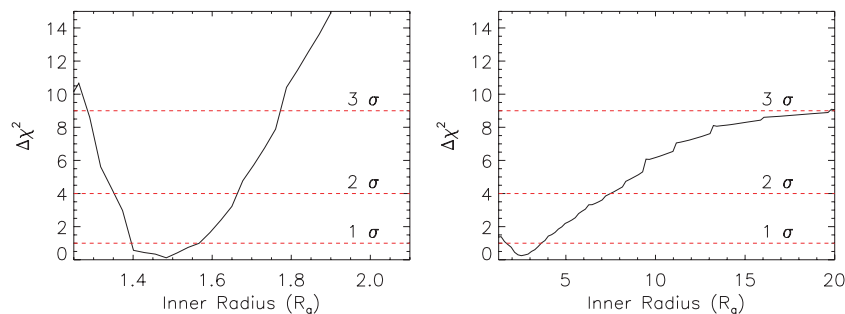
Figure 18. Left-hand panel: goodness-of-fit variation as a function of inner radius for J1655−40. Right-hand panel: similar to the left but for J1753.5−0127.

found to be below $\approx 10 r_g$ and in all cases they are consistent with extending to the ISCO down to luminosities of $\sim 5 \times 10^{-4} L_{\rm Edd}$. The lack of constraints in the physical parameters (mass, distance and inclination) of J17497 and J1817 results in a large uncertainty in the derived inner radii; however, even when extreme values are used for these parameters, the results are still consistent with lack of disc truncation further than $\sim 100 r_g$ for these sources. All results presented above are robust to the choice of MCD component used. We emphasize here that throughout this work we have used the largest range in the physical parameters for the various sources obtained from the literature. Even with this conservative choice, we have shown that the 3σ upper limit on the disc radius, as obtained from the flux of the thermal component, does not require large disc truncation.

It is interesting to note that in all sources presented here the disc temperature are found to be below ≈ 0.3 keV, with the majority clustered at ≈ 0.2 keV. The disc flux found at these low accretion rates results in an insignificant amount of flux visible to *RXTE* PCA, with its effective low energy cut-off of ≈ 3 keV. Zdziarski & Gierliński (2004) investigated the state transition of GX 339−4 using *RXTE*. Their fig. 10 shows a sharp change in the inner radius – obtained via the disc flux methodology – during the change to the low-hard state. Similar conclusions based on the apparent change in the normalization of the DISKBB model have been presented by Belloni et al. (1997) for the BHB GRS J1915+105 again using *RXTE PCA* data above 2.5 keV.

Using a further MCD model where the inner radius is a free parameter, we investigated in Section 3.4 the possibility that the thermal component originates further than $100 r_g$ as expected from ADAF models. Fig. 8 shows that this conviction was excluded for all sources other than J17497 and J1817. Our conclusions depend on the maximum plausible value for the spectral hardening factor f. Hardening arises at higher photon energies where the opacity of the disc atmosphere is lower and photons emerge from deeper layers

where gas is hotter. Approximately, $f = T/T_{\rm eff} \simeq \tau^{1/4}$, where τ is the Thomson depth of the layer from which the photons emerge (Ross, Fabian & Mineshige 1992; Davis, Done & Blaes 2006 in the high τ limit). The photons then need to scatter out through the outer layers which are cooler than where they formed. This introduces a Compton downscattering break in the spectrum at an energy $\epsilon \sim m_{\rm e} c^2/\tau^2$. There are therefore two competing effects: seeing to deeper layers making the spectrum harder and Compton downscattering by intervening material making it softer. The maximum value of f occurs before the effects balance, which is at $f = (m_{\rm e} c^2/\epsilon)^{1/8}$. Therefore, if we take $\epsilon \sim 0.5$ keV to mark the harder part of the thermal emission, $f < 2.4$. An absolute limit will depend on exactly which part of the spectrum is being fitted. We consider that $f = 3$ is a conservative upper limit.

The high significance of the thermal component in the various sources studied here, coupled with the total flux and temperature range (≈ 0.15–0.3 keV) obtained from MCD models such as DISKBB, strongly argues for the presence of a standard optically thick accretion disc extending close to the ISCO.

4.2 Constraints from reflection signatures

Further evidence for an optically thick disc extending to the ISCO in the low-hard state comes from the presence of a broad, skewed Fe Kα line and strong reflection hump observed in five out of the eight sources presented. These reflection features arise due to reprocessing of hard X-ray by the cooler accretion disc (Ross & Fabian 1993). In the region surrounding a black hole, the strong gravitational potential causes these reflection features to become highly distorted, with the degree of distortion depending on how far from the black hole the emitting region is located. Therefore, the shape of the prominent iron Kα line can give a direct indication of the radius of the reflection material from the black hole (Fabian et al. 1989, 2000; Laor 1991).

Section 3.5 shows the reflection signatures of five sources. It is clear from Figs 9 to 18 that in all cases investigated the inner radius of emission, as obtained from the degree of gravitational blurring of these features, is consistent with the ISCO down to luminosities of $\sim 1.5 \times 10^{-3} L_{\mathrm{Edd}}$. For GX 339$-$4, J1650, J1655 and J1753, the results further imply that the central source is a rotating, Kerr black hole with the disc extending to less than $6r_{\mathrm{g}}$ at 5σ confidence in most cases. This is in agreement with results found from prior studies in various states (GX 339$-$4: Reis et al. 2008; Miller et al. 2008. J1650: Miller et al. 2002; Miniutti et al. 2004. J1655: Díaz Trigo et al. 2007; Reis et al. 2009b. J1753: Miller et al. 2006; Reis et al. 2009b) which supports the idea that the emitting area is not changing between these states. A non-rotating, Schwarzschild black hole is not ruled out for Cyg X-1; however, a disc with an edge at greater than $20r_{\mathrm{g}}$ is excluded at over 5σ.

For four out of the five sources, where an iron Kα emission line is seen, the equivalent width, as measured from the LAOR line component, is found to be greater than 70 eV at the 90 per cent level of confidence. It was shown by George & Fabian (1991) that for a neutral, optically thick accretion disc extending to the ISCO the reflection fraction $R \sim W_{\mathrm{K}\alpha}/180\,\mathrm{eV}$. Beloborodov (1999) later showed that reflection fractions as low as ≈ 0.3 can be achieved by the mild relativistic bulk motion of a corona away from an accretion disc. Based on these arguments, it can be seen that $W_{\mathrm{K}\alpha} \gtrsim 60\,\mathrm{eV}$ is still consistent with originating in an accretion disc extending to the ISCO.

4.3 Radio jets and disc truncation

The sample investigated here covers a large range of luminosities from ≈ 0.05 to 1.5 per cent of the Eddington limit; however, this is still an order of magnitude larger than the predicted quiescent transition value of $\approx 4 \times 10^{-5} L_{\mathrm{Edd}}$ (Gallo, Fender & Pooley 2003) below which the black holes are thought to be jet dominated. The presence of radio jets is usually associated with systems in the low-hard state (see e.g. Fender 2001, 2006), and it has at times been attributed to a receding (ejected?) inner disc (see e.g. Belloni et al. 1997). In this scenario, the inner part of the accretion flow in the low-hard state is advection dominated. The radio jet is then quenched when the inner region is filled by an accretion disc, as is the case in the high-soft state. Our findings suggest that jet production is not initiated at the point where the accretion disc starts to recede. Another possibility for the production of jets could be due to a change in the ratio of the energy dissipated in a corona to that dissipated in the disc between the various states, an intrinsic change in the mass accretion rate through the disc or even changes in the vertical scaleheight close to the central black hole.

It is still possible that below the luminosities studied here an advection flow might be present at which point the disc could be truncated. This ADAF solution is usually agreed to be the dominant emission process in the Galactic Centre source Sgr A* (Narayan, Yi & Mahadevan 1995; Narayan et al. 1998) as well as various low-luminosity active galactic nuclei (LLAGN; Di Matteo et al. 2000, 2003). However, an alternative, jet-dominated accretion flow explanation has also been successfully applied to these sources (Sgr A*: Falcke & Biermann 1999; Falcke & Markoff 2000; LLAGNs: Falcke et al. 2000). In order to test whether the accretion disc recedes at luminosities below those observed here, as well as the profound connection between accretion disc and jets, we strongly encourage deeper observations of black holes in the low-hard and quiescent

states from instruments such as *XMM–Newton*, *Suzaku* and in the future *IXO*.

5 CONCLUSION

In this paper, we have investigated a sample of stellar mass black holes in the canonical low-hard state. By systematically analysing their X-ray spectrum, we have found that in all cases the accretion disc is consistent with being at the ISCO down to luminosities as low as $\approx 5 \times 10^{-4} L_{\mathrm{Edd}}$. The main points and implication of this paper are summarized as follows.

(1) In all sources investigated, the presence of an accretion disc is required at the 5σ level of confidence. The temperature and flux of this thermal component are consistent with the $L \propto T^4$ relation and with a geometrically thin, optically thick accretion disc extending to the ISCO.

(2) The presence of reflection features and predominantly an iron Kα emission line with an equivalent width greater than ~ 70 eV is detected in half of the sample. In all these cases, the broadness of the reflection features further suggests that the accretion disc is not highly truncated.

(3) Our findings suggest that transition to the low-hard state is driven by changes in the corona (perhaps related to jet formation) and not changes in the accretion disc.

(4) Jet production is not initiated at the point where the disc recedes.

(5) Furthermore, we suggest the following strong and weak observation criteria for disc truncation:

(i) the data must be able to rule out both a broad iron Kα line with an equivalent width $\gtrsim 60$ eV and an effective disc temperature consistent with $L \propto T^4$ or

(ii) the data must be able to rule out either a broad iron Kα line with an equivalent width $\gtrsim 60$ eV or an effective disc temperature consistent with $L \propto T^4$.

Whilst the number of sources presented here is small, there is a general trend that when the accretion disc is statistically required the data suggest that the disc in the low-hard state can remain at the ISCO. This result is contrary to the lore that the accretion disc in the low-hard state is truncated at hundreds of gravitational radii, as required in the strong-advection-dominated interpretation.

REFERENCES

Arnaud K. A., 1996, in Jacoby G. H., Barnes J., eds, ASP Conf. Ser. Vol. 101, Astronomical Data Analysis Software and Systems V. Astron. Soc. Pac., San Francisco, p. 17
Barrio F. E., Done C., Nayakshin S., 2003, MNRAS, 342, 557
Beloborodov A. M., 1999, ApJ, 510, L123
Belloni T., Mendez M., King A. R., van der Klis M., van Paradijs J., 1997, ApJ, 479, L145

Brenneman L. W., Reynolds C. S., 2006, ApJ, 652, 1028

Brocksopp C. et al., 2006, MNRAS, 365, 1203

Caballero-Garcia M., Fabian A. C., 2009, MNRAS, in press (arXiv: 0910.2418)

Cackett E. M. et al., 2008, ApJ, 674, 15

Cadolle Bel M. et al., 2007, ApJ, 659, 549

Davis S. W., Blaes O. M., Hubeny I., Turner N. J., 2005, ApJ, 621, 372

Davis S. W., Done C., Blaes O. M., 2006, ApJ, 647, 525

Díaz Trigo M., Parmar A. N., Miller J. M., Kuulkers E., Caballero-García M. D., 2007, A&A, 462, 657

Di Matteo T., Celotti A., Fabian A. C., 1999, MNRAS, 304, 809

Di Matteo T., Quataert E., Allen S. W., Narayan R., Fabian A. C., 2000, MNRAS, 311, 507

Di Matteo T., Allen S. W., Fabian A. C., Wilson A. S., Young A. J., 2003, ApJ, 582, 133

Done C., Gierlinski M., 2006, MNRAS, 367, 659

Done C., Davis S. W., 2008, ApJ, 683, 389

Dotani T. et al., 1997, ApJ, 485, L87

Dovciak M., Karas V., Yaqoob T., 2004, ApJ, 153, 205

Esin A. A., McClintock J. E., Narayan R., 1997, ApJ, 489, 865

Esin A., McClintock J. E., Drake J. J., Garcia M. R., Haswell C. A., Hynes R. I., Muno M. P., 2001, ApJ, 555, 483

Fabian A. C., Rees M. J., Stella L., White N. E., 1989, MNRAS, 238, 729

Fabian A. C., Iwasawa K., Reynolds C. S., Young A. J., 2000, PASP, 112, 1145

Fabian A. C. et al., 2009, Nat, 459, 540

Falcke H., Biermann P. L., 1999, A&A, 342, 49

Falcke H., Markoff S., 2000, A&A, 362, 113

Falcke H., Nagar N. M., Wilson A. S., Ulvestad J. S., 2000, ApJ, 542, 197

Fender R. P., 2001, MNRAS, 322, 31

Fender R. P., 2006, in Lewin W. H. G., van der Klis M., eds, Compact Stellar X-ray Sources. Cambridge Univ. Press, Cambridge, p. 381

Frontera F. et al., 2001, ApJ, 561, 1006

Gallo E., Fender R. P., Pooley G. G., 2003, MNRAS, 344, 60

Gallo E., Corbel S., Fender R. P., Maccarone T. J., Tzioumis A. K., 2004, MNRAS, 347, L52

Gelino D. M., Balman S., Kiziloglu U., Yilmaz A., Kalemci E., Tomsick J. A., 2006, ApJ, 642, 438

George I. M., Fabian A. C., 1991, MNRAS, 249, 352

Gierlinski M., Zdziarski A. A., Poutanen J., Coppi P. S., Ebisaka K., Johnson W. N., 1999, MNRAS, 309, 496

Gierlinski M., Done C., Page K., 2008, MNRAS, 388, 753

Greene J., Bailyn C. D., Orosz J. A., 2001, Apj, 554, 1290

Hiemstra B., Soleri P., Mendez M., Belloni T., Mostafa R., Wijnands R., 2009, MNRAS, 394, 2080

Hjellming R. M., Rupen M. P., 1995, Nat, 375, 464

Homan J., Wijnands R., Kong A., Miller J. M., Rossi S., Belloni T., Lewin W. H. G., 2006, MNRAS, 366, 235

Hynes R. I., Steeghs D., Casares J., Charles P. A., O'Brian K., 2003, ApJ, 583, L95

Koyama K. et al., 2007, PASJ, 59, S23

Laor A., 1991, ApJ, 376, 90

Liu B. F., Taam R. E., Meyer-Hofmeister E., Meyer F., 2007, ApJ, 671, L695

McClintock J. E., Remillard R. A., 2006, in Lewin W. H. G., van der Klis M., eds, Compact Stellar X-ray Sources. Cambridge Univ. Press, Cambridge, p. 157

McClintock J. E. et al., 2001, ApJ, 555, 477

Maccarone T. J., 2003, A&A, 409, 697

Makishima K. et al., 2008, PASJ, 60, 585

Markoff S., Nowak M. A., 2004, ApJ, 609, 972

Markoff S., Nowak M. A., Wilms J., 2005, ApJ, 635, 1203

Martin R. G., Tout C. A., Pringle J. E., 2008a, MNRAS, 387, 188

Martin R. G., Reis R. C., Pringle J. E., 2008b, MNRAS, 391, L15

Massey P., Johnson K. E., Degioia-Eastwood K., 1995, ApJ, 454, 151

Merloni A., Fabian A. C., 2001, MNRAS, 332, 165

Merloni A., Fabian A. C., 2002, MNRAS, 332, 165

Merloni A., Fabian A. C., Ross R. R., 2000a, MNRAS, 313, 193

Merloni A., Di Matteo T., Fabian A. C., 2000b, MNRAS, 318, L15

Miller J. M., 2007, ARA&A, 45, 441

Miller J. M., 2009, Astron. Tel., 1966, 1

Miller J. M. et al., 2002, ApJ, 570, L69

Miller J. M. et al., 2004, ApJ, 606, L131

Miller J. M., Fabian A. C., Nowak M. A., Lewin W. H. G., 2005, tmgm.meet., 1296M

Miller J. M., Homan J., Steeghs D., Rupen M., Hunstead R. W., Wijnands R., Charles P. A., Fabian A. C., 2006a, ApJ, 653, 525

Miller J. M., Homan J., Miniutti G., 2006b, ApJ, 652, L113

Miller J. M. et al., 2008, ApJ, 679, L113

Miller J. M., Reynolds C. S., Fabian A. C., Miniutti G., Gallo L. C., 2009a, ApJ, 697, 900

Miller J. M., Cackett E. M., Reis R. C., 2009b, ApJ, 707, 77

Miniutti G., Fabian A. C., Miller J. M., 2004, MNRAS, 351, 466

Mitsuda K. et al., 1984, PASJ, 36, 741

Muñoz-Darias T., Casares J., Martínez-Pais I. G., 2008, MNRAS, 385, 2205

Murdin P., Webster L. B., 1971, Nat, 233, 110

Narayan R., Yi I., 1995, ApJ, 452, 710

Narayan R., Mahadevan R., Grindlay J. E., Popham R. G., Gammie C., 1998, ApJ, 492, 554

Narayan R., Yi I., Mahadevan R., 1995, Nat, 374, 623

Orosz J. A., McClintock J. E., Remillard R. A., Corbel S., 2004, ApJ, 616, 376

Paizis A. et al., 2007, ApJ, 657, L109

Paizis A. et al., 2008, PASJ, in press (arXiv:0811.2663)

Ramadevi M. C., Seetha S., 2007, MNRAS, 378, 182

Reis R. C., Fabian A. C., Ross R. R., Miniutti G., Miller J. M., Reynolds C., 2008, MNRAS, 387, 1489

Reis R. C., Miller J. M., Fabian A. C., 2009a, MNRAS, 395, L52

Reis R. C., Fabian A. C., Ross R. R., Miller J. M., 2009b, MNRAS, 395, 1257

Reis R. C., Fabian A. C., Young A. J., 2009c, MNRAS, 399, L1

Remillard R., Levine A. M., Morgan E. H., Markwardt C. B., Swank J. H., 2006, Astron. Tel., 714, 1

Romero G. E., Kaufman Bernado M. M., Mirabel I. F., 2002, A&A, 393, L61

Ross R. R., Fabian A. C., 1993, MNRAS, 261, 74

Ross R. R., Fabian A. C., 2005, MNRAS, 358, 211

Ross R. R., Fabian A. C., Mineshige S., 1992, MNRAS, 258, 189

Ross R. R., Fabian A. C., Young A. J., 1999, MNRAS 306, 461

Rossi S., Homan J., Miller J. M., Belloni T., 2005, MNRAS, 360, 763

Rykoff E. S., Miller J. M., Steeghs D., Torres M. A. P., 2007, ApJ, 666, 1129 (R07)

Sala G., Greiner J., Ajello M., Bottacini E., Haberl F., 2007, A&A, 473, 561

Shakura N. I., Sunyaev R. A., 1973, A&A, 24, 337

Shapiro S. L., Lightman A. P., Eardley D. M., 1976, ApJ, 204, 187

Shaposhnikov N., Titarchuk L., 2009, ApJ, 699, 453

Shimura T., Takahara F., 1995, ApJ, 445, 780

Stirling A. M., Spencer R. E., de la Force C. J., Garrett M. A., Fender R. P., Ogley R. N., 2001, MNRAS, 327, 1273

Sunyaev R. A., Titarchuk L. G., 1980, A&A, 86, 121

Taam R. E., Liu B. F., Meyer F., Meyer-Hofmeister E., 2008, ApJ, 688, 527

Takahashi K., Inoue H., Dotani T., 2001, PASJ, 53, 1171

Takahashi H. et al., 2008, PASJ, 60S, 69

Tanaka Y. et al., 1995, Nat, 375, 659

Tananbaum H., Gursky H., Kellogg E., Giacconi R., Jones C., 1972, ApJ, 177, L5

Thorne K. S., 1974, ApJ, 191, 507

Tomsick J. A. et al., 2008, ApJ, 680, 593

Torres D. F., Romero G. E., Barcons X., Lu Y., 2005, ApJ, 626, 1015

Wagner R. M., Foltz C. B., Shahbaz T., Casares J., Charles P. A., Starfield S. G., Hewett P., 2001, ApJ, 556, 42

Wilms J., Nowak M. A., Dove J. B., Fender R. P., Di Matteo T., 1999, ApJ, 522, 460

Young A. J., Fabian A. C., Ross R. R., Tanaka Y., 2001, MNRAS, 325, 1045

Zdziarski A. A., Gierlinski M., 2004, Prog. Theor. Phys. Suppl., 155, 99

Zdziarski A. A., Gierlinski M., Mikolanjewska J., Wardzinski G., Smith D. M., Harmon A., Kitamoto S., 2004, MNRAS, 351, 791

Zimmerman E. R., Narayan R., McClintock J. E., Miller J. M., 2005, ApJ, 618, 832

Ziolkowski J., 2005, MNRAS, 358, 851

Zurita C., Durant M., Torres M. A. P., Shahbaz T., Casares J., Steeghs D., 2008, ApJ, 681, 1458

This paper has been typeset from a TEX/LATEX file prepared by the author.